Unraveling hallmark suitability for staging pre- and post-implantation stem cell models

Constance Onfray, Simon Chevolleau, Eva Moinard, Océane Girard, Kasturi Mahadik, Ryan Allsop, Grigorios Georgolopoulos, Rob Lavigne, Ophélie Renoult, Irène Aksoy, et al.

Cell Reports

Unraveling hallmark suitability for staging pre- and post-implantation stem cell models

Graphical abstract

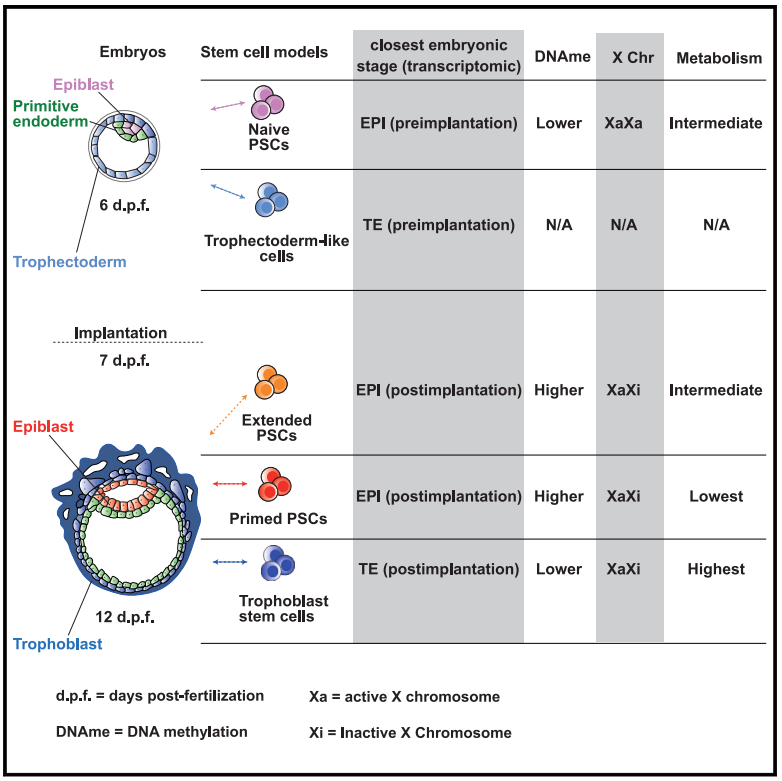

Highlights

- Comparison of hTSCs, hTELCs, primed hPSCs, naive hPSCs, and hEPSCs
- hEPSCs have DNAme levels and X activity similar to primed hPSCs
- hEPSCs have a higher metabolic activity than hPSCs
- hTSCs have the highest metabolic activity of all cell types measured

Authors

Constance Onfray, Simon Chevolleau, Eva Moinard, ..., Vincent Pasque, Claire Rougeulle, Laurent David

Correspondence

laurent.david@univ-nantes.fr

In brief

Onfray et al. report the comparison of hTSCs, hTELCs, and primed, extended, and naive hPSCs by transcriptomics, proteomics, DNAme quantification, X, and metabolic activity. TELCs have features of trophectoderms, while TSCs represent post-implantation trophoblasts. hEPSCs are clearly primed cells but display a higher metabolic and clonogenic potential than regular primed PSCs.

Onfray et al., 2024, Cell Reports *43*, 114232
May 28, 2024
https://doi.org/10.1016/j.celrep.2024.114232

CellPress

Cell Reports

CellPress
OPEN ACCESS

Report

Unraveling hallmark suitability for staging pre- and post-implantation stem cell models

Constance Onfray,[1] Simon Chevolleau,[1] Eva Moinard,[1] Océane Girard,[1] Kasturi Mahadik,[2] Ryan Allsop,[3] Grigorios Georgolopoulos,[3] Régis Lavigne,[7,8] Ophélie Renoult,[5] Irene Aksoy,[6] Elsa Lemaitre,[4] Philippe Hulin,[4] Jean-François Ouimette,[2] Thomas Fréour,[1,9,10] Claire Pecqueur,[5] Charles Pineau,[7,8] Vincent Pasque,[3] Claire Rougeulle,[2] and Laurent David[1,4,11,*]

[1]Nantes Université, CHU Nantes, Inserm, CR2TI, 44000 Nantes, France
[2]Université Paris Cité, CNRS, Epigenetics and Cell Fate, 75013 Paris, France
[3]KU Leuven – University of Leuven, Department of Development and Regeneration, Leuven Institute for Single Cell Omics and Leuven Stem Cell Institute, Herestraat 49, 3000 Leuven, Belgium
[4]Nantes Université, CHU Nantes, Inserm, CNRS, BioCore, SFR Bonamy, 44000 Nantes, France
[5]Nantes Université, CNRS, Inserm, CRCI2NA, 44000 Nantes, France
[6]University Lyon, Université Lyon 1, Inserm, Stem Cell and Brain Research Institute U1208, 69500 Bron, France
[7]University Rennes, Inserm, EHESP, Irset (Institut de Recherche en Santé, Environnement et Travail) – UMR_S 1085, 35000 Rennes, France
[8]University Rennes, CNRS, Inserm, Biosit UAR 3480 US_S 018, Protim Core Facility, 35000 Rennes, France
[9]Department of Obstetrics, Gynecology and Reproductive Medicine, Dexeus University Hospital, 08028 Barcelona, Spain
[10]CHU Nantes, Service de Biologie de la Reproduction, 44000 Nantes, France
[11]Lead contact
*Correspondence: laurent.david@univ-nantes.fr
https://doi.org/10.1016/j.celrep.2024.114232

SUMMARY

The advent of novel 2D and 3D models for human development, including trophoblast stem cells and blastoids, has expanded opportunities for investigating early developmental events, gradually illuminating the enigmatic realm of human development. While these innovations have ushered in new prospects, it has become essential to establish well-defined benchmarks for the cell sources of these models. We aimed to propose a comprehensive characterization of pluripotent and trophoblastic stem cell models by employing a combination of transcriptomic, proteomic, epigenetic, and metabolic approaches. Our findings reveal that extended pluripotent stem cells share many characteristics with primed pluripotent stem cells, with the exception of metabolic activity. Furthermore, our research demonstrates that DNA hypomethylation and high metabolic activity define trophoblast stem cells. These results underscore the necessity of considering multiple hallmarks of pluripotency rather than relying on a single criterion. Multiplying hallmarks alleviate stage-matching bias.

INTRODUCTION

The discovery and popularization of organoid, complex stem cell-based models, calls for a strong effort of characterization and standardization. Community efforts have led to the revision of ISSCR standards for basic stem cell research. While most of the community's effort has been focused on primed pluripotency, the recent development of blastoids and other stem cell models of peri-implantation demonstrates the importance of applying the same efforts to all stem cell models, including peri-implantation models.[1]

A flurry of cellular systems has been developed to model the different lineages of the human embryo. In 1998, pluripotent stem cells (PSCs) were derived from human blastocysts[2] and were later shown to correspond to the post-implantation epiblast (10–14 dpf), hence to a primed state of pluripotency. Culture conditions to capture cells corresponding to pre-implantation epiblast (6–9 dpf) were later developed, allowing naive pluripotent stem cells to be derived from human blastocysts.[3–7] Later work then generated naive pluripotent stem cells (NPSCs) by resetting primed pluripotent stem cells (PPSCs) or through reprogramming using OCT4, SOX2, KLF4, MYC (OSKM).[8–13]

NPSCs have the closest transcriptomic profile to human pre-implantation epiblasts. They express specific proteins such as KLF17, DNMT3L, and DPPA5.[9] They are hypomethylated and have a higher metabolic activity compared to PPSCs. Female cell lines also have both X chromosomes active.[4,9,14–22] All these characterization efforts led to the establishment of consensus hallmarks for the assessment of naive pluripotency.[23] Recently, new markers have been added to the previously established hallmarks of naive pluripotency: the ability to make human-animal chimeras, to differentiate into the trophoblast lineage, and to form blastoids.[7,12,22,24–32]

An additional state of pluripotency has been captured *ex vivo* and reported to contribute to chimeras, although at low efficiency, and to convert into extra-embryonic cells: extended PSCs or

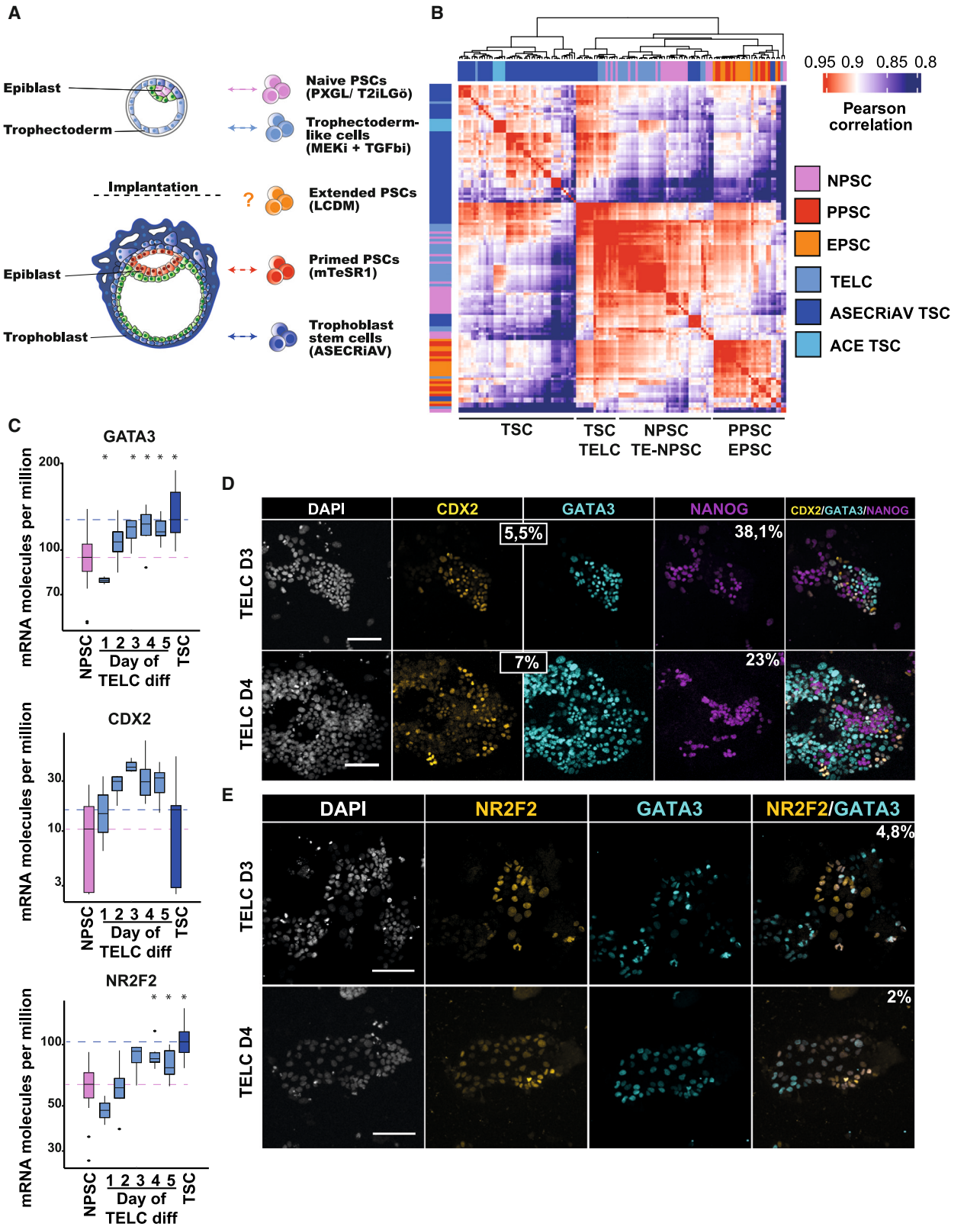

(legend on next page)

EPSCs.[25,32–35] It has been proposed that these pluripotent stem cells with extended or expanded potential resemble 2C-like cells and represent a new, more potent state of stemness.[31,33,35] However, several groups have pointed out the limit of the chimera experiments performed in EPSC studies both in mouse and human.[36,37] Since EPSCs are not actually colonizing tissues, one could propose that these cells have the ability to survive in an ectopic environment but do not actually chimerize with the host embryos. Additionally, these cells have not been properly benchmarked using naive pluripotency hallmarks.

Trophoblast stem cells (TSCs) have recently been derived from human blastocyst but also from first trimester placenta.[38] Our team and others also observed that naive PSCs can engage into the trophoblast fate and convert into TSCs.[25,27,39] An alternative culture medium to the original ASECRiAV medium[38] that enables maintaining TSCs in culture was also developed: ACE medium.[40] While TSCs have been proposed to correspond to cytotrophoblasts emerging around 7 to 9 days post fertilization (d.p.f.),[25] the validation mostly relied on transcriptomic analysis. Further work is needed to precisely characterize TSCs and their correspondence with the human embryo but also to determine the correspondence between cells cultured in ASECRiAV and ACE medium. In addition, pre-implantation trophectoderm engagement of naive PSCs has been observed upon inhibition of NODAL and ERK pathways,[40,41] but again, the cells were mostly characterized at the transcriptomic level.

The wide range of stem cell models gives the unique opportunity to clarify which hallmark is associated with which lineage and developmental stage. Here, we have characterized human EPSCs and TSCs in parallel with NPSCs and PPSCs through analyses of transcriptomic, proteomic, epigenetic, and metabolic features. Parallel comparison of peri-implantation stem cell models over different characteristics will significantly contribute to the establishment of standards for these models, as previously done for primed pluripotency.

RESULTS

Transcriptomic comparison of pluripotent and trophoblast stem cell models

In order to compare transcriptomic features of pre- and post-implantation models, we co-analyzed RNA-seq datasets from NPSCs, PPSCs, EPSCs, TSCs, and trophectoderm-like cells (TELCs) (Figures 1A, 1B, and S1A). To avoid biases associated with sequencing platforms, we obtained RNA directly from the groups that generated the models: NPSCs,[6] ACE-TSCs,[40] and placenta- and blastocyst-derived ASECRiAV-TSCs.[38] And, we compared them to 6 ASECRiAV-TSCs lines generated in house: 3 induced TSCs from somatic cells and 3 converted TSCs from NPSCs. We also included NPSCs undergoing TSC conversion[42] and TELCs generated through differentiation of NPSCs treated with A8301 and PD0325901 (AP) up to 6 days, as published in Guo et al., 2021.[41] Finally, we included 2 EPSC lines generated in house,[25] 4 PPSC lines (3 in-house and H9 hESCs), and 7 NPSC lines (6 in-house[9] and HNES1 line[6]; Table S3).

We performed a Pearson correlation analysis on all samples that revealed 4 main groups of samples: (1) all TSCs, from Okae et al. and Castel et al., later mentioned as ASECRiAV-TSCs, together with TSCs from Io et al., later referred to as ACE-TSCs; (2) some TSCs together with TELCs; (3) all NPSCs together with some intermediates of TELC differentiation, referred as TE-NPSCs; and (4) EPSCs together with PPSCs (Figure 1B). We also performed a correlation analysis after grouping samples per culture condition, which confirmed correlation between TELCs with both TSCs and NPSCs (Figure S1A).

TELCs recapitulate human TE specification molecular aspects but are heterogeneous

TELCs have been proposed to recapitulate human TE maturation.[41] To further study this aspect, we analyzed three markers of TE fate progression that we recently described in human embryos: GATA3, the earliest marker of TE specification,[43] and CDX2, which comes up at B3 blastocyst stage,[28,44] followed by NR2F2 upon TE maturation at the polar side.[45] We measured the expression levels of these key markers of trophoblastic fate progression using bulk RNA sequencing. mRNA quantification showed an increase of expression upon differentiation relative to the control NPSC from 48 h after induction of differentiation for GATA3 and CDX2, a peak of expression 72 h after induction of differentiation for CDX2, and an increase of expression relative to the control NPSC 72 h after induction of differentiation for NR2F2 (Figure 1C). To verify that the proteins were expressed, we performed immunofluorescence (IF) analysis, which confirmed the presence of nuclear staining in some colonies (Figures 1D and 1E). IF analysis revealed that the differentiation was heterogeneous with an important proportion of cells still expressing the

Figure 1. Transcriptomic analysis of human PSC, EPSC, NPSC, TSC, and TELC lines

(A) Schematic representation of stem cell types tested and their proposed developmental stage counterpart along with the culture medium in which they are typically cultured.

(B) Heatmap of Pearson correlation coefficients of PSC, EPS, NPSC, and TSC lines along with TELC differentiation from NPSC and TSC lines from Io et al. study samples are clustered from the Euclidian distance of correlation by a hierarchical clustering using Ward's method.

(C) Gene expression levels of indicated lineage markers are shown for NPSCs and the different days of differentiation of NPSCs into TELC and TSC lines. The NPSC and TSC lines are included as control. Expression levels are given as number of transcripts per million mRNA molecules. In each boxplot, the top and bottom of the box represent the third and first quartile, respectively; the band represents the median (second quartile); and error bars show the interquartile range (IQR) (lower bound: Q1 – 1.5 × IQR; upper bound: Q3 + 1.5 × IQR). *p* values from differential gene expression analysis were re-used for boxplots. Asterisks indicate statistical significance of the difference compared to NPSCs: $*p < 0.05$.

(D) Immunofluorescence images of day 3 and day 4 of TELC differentiation from NPSCs stained for trophoblast-associated transcription factors GATA3 and CDX2 and pluripotency-associated transcription factor NANOG. Quantification of cells positives for both GATA3 and CDX2 or positive for NANOG is indicated for each day. Nuclei were stained with DAPI. Scale bar represents 100 μm.

(E) Immunofluorescence images of day 3 and day 4 of TELC differentiation from NPSCs stained for trophoblast-associated transcription factors GATA3 and NR2F2. Quantification of cells positive for both GATA3 and NR2F2 is indicated for each day. Nuclei were stained with DAPI. Scale bar represents 100 μm.

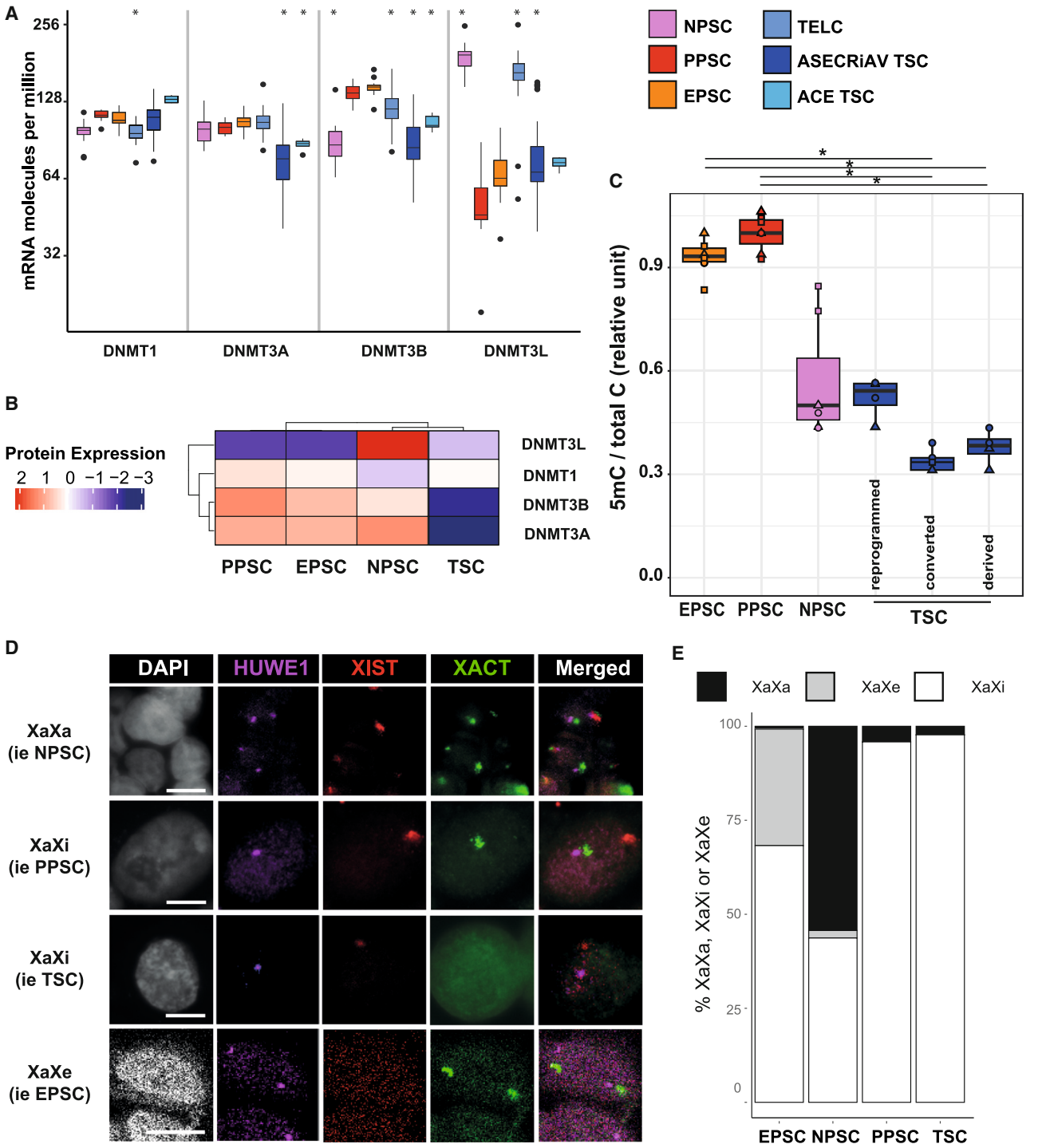

Figure 2. DNA methylation and X chromosome coating of PSCs, EPSCs, NPSCs, and TSCs

(A) Gene expression levels of indicated genes are shown for NPSC, PPSC, EPSC, TELC, and TSC lines. The NPSC and PPSC lines are included as control. Expression levels are given as number of transcripts per million mRNA molecules. In each boxplot, the top and bottom of the box represent the third and first quartile, respectively; the band represents the median (second quartile); and error bars show the interquartile range (IQR) (lower bound: Q1 – 1.5 × IQR; upper bound: Q3 + 1.5 × IQR). *p* values from differential gene expression analysis were re-used for boxplots. Asterisks indicate statistical significance of the difference compared to PPSCs: $^{*}p < 0.05$.

(B) Heatmap of relative expression of DNMT1, DNMT3A, DNMT3B, and DNMT3L proteins.

(legend continued on next page)

pluripotency marker NANOG (Figure S1A). We conclude that cells acquire GATA3 first, and based on transcriptomic data, CDX2 second, and NR2F2 last, as in blastoids.[28] Additionally, immunofluorescence quantification showed that a significant proportion of cells (30%–40%) did not engage toward the TE fate, which is consistent with recent reports.[46,47] Given the high heterogeneity of TELCs in our hands, we excluded this model from further population-based analysis.

DNA methylation levels are lower in TSCs and NPSCs compared to PSCs and EPSCs

As a proxy to characterize the chromatin features of stem cell models for human peri-implantation development, we analyzed expression levels of the DNMT gene family. This revealed that DNMT3L is mostly expressed in NPSCs[47] and that DNMT3B, responsible for DNA methylation, is more expressed in PPSCs and EPSCs. Interestingly, TSCs have the lowest expression of DNMT3A and have low expression of DNMT3B, like NPSCs. However, TSCs express low levels of DNMT3L, like PPSCs. On another hand, EPSCs have a similar profile to PPSCs (Figure 2A). To validate our transcriptomic data, we used mass spectrometry data as an orthogonal validation dataset. To do so, we acquired a proteomic profile of EPSCs and PPSCs to complete our previously described dataset of NPSCs and TSCs.[48] Mass spectrometry data independent analysis detected, respectively, 8,740, 8,659, and 9,141 proteins in NPSCs, PPSCs, and EPSCs. An in-depth analysis was performed on the peptide score, reflecting the sum of areas under the curve for all the fragments corresponding to one peptide precursor. This analysis reflects protein expression. Protein expression of DNMT1, DNMT3A, DNMT3B, and DNMT3L by mass spectrometry confirmed the transcriptomic analysis, associating the EPSCs with PPSCs and confirming the low levels of DNMT3A, DNMT3B, and DNMT3L in TSCs (Figure 2B).

We then quantified global DNA methylation levels, as it has proven to be a robust way to assess naive vs. primed pluripotency.[4,9,21–23] We quantified 5-methylcytosine (5mC) by mass spectrometry and showed that cells are organized in two samples groups. On one hand, we identified PPSCs and EPSCs linking EPSCs with primed pluripotency (Figures 2C and S2A). On the other hand, NPSCs and TSCs were hypomethylated when compared to PPSCs and EPSCs (Figure 2C). This complements the observation by Okae and collaborators that TSCs are globally hypomethylated relative to cytotrophoblasts.[26,38] Altogether, our investigation precisely specifies the relative methylation levels between all peri-implantation stem cell models and associate EPSCs with the primed state of pluripotency.

TSCs and EPSCs have one inactivated X chromosome, contrasting with NPSCs

The X chromosome activity status has been shown as one of the most stringent criteria that distinguishes NPSCs and PPSCs, with female NPSCs carrying 2 active X chromosomes (Xa), whereas female PPSCs are characterized by the presence of one active and one inactive X (Xi).[9,16] This can be monitored by RNA-fluorescence in situ hybridization (FISH) of X-linked genes such as HUWE1 or XACT that demarks X transcriptional activity.[15,16] RNA-FISH for the long non-coding RNA XIST, the trigger of XCI, can also be informative, although in NPSCs, presence of XIST is unlinked from silencing.[16] In addition, progressive loss of XIST expression and other XCI hallmarks occurs spontaneously upon culturing PPSCs, a process called XCI erosion[49,50]; erosion is, for example, accompanied by the re-expression of certain genes on the X including XACT. Erosion of XCI has been associated with the presence of GSK3 inhibitor in the culture medium.[51] As we are using culture medium with GSK3 inhibitor, we included the analysis of XACT lncRNA to take this potential bias into account in our analysis.

Analysis and quantification of XIST, XACT, and HUWE1 patterns in NPSCs, PPSCs, EPSCs, and TSCs allowed us to determine the activity status of each chromosome (Table S3B). The XaXa status is determined by bi-allelic expression of HUWE1 and XACT associated with the presence of XIST from at least one chromosome. The XaXi status is defined by monoallelic expression of HUWE1 together with XIST accumulation from the other X chromosome. Finally, the XaXe status is inferred from co-presence of XACT and HUWE1 on both chromosomes and lack of XIST expression (Table S3B) (Figure 2D). We observed that NPSCs display 2 active Xs in more than 50% of the cells (Figures 2E and S1D). On the other hand, TSCs, like PPSCs, show inactivation of one X chromosome in more than 80% of the cells, corroborating recent findings obtained in trophoblast organoids.[52] Of note, we observed that TSCs do not express XACT, in line with the hypothesis of Vallot et al. that XACT is lost upon TE specification in pre-implantation embryos[16]. Finally, EPSCs are either XaXi or XaXe (Figures 2D and 2E). Of note, one female EPSC line was massively XaXe, whereas the other one was XaXi (Figure S1D). In all cases, EPSCs are in a post-XCI state, confirming their association with the primed state of pluripotency. Altogether, our analysis revealed distinct X chromosome activity status in peri-implantation stem cell models that resembles their *in vivo* counterpart.

Metabolism-related genes distinguish EPSCs from PPSCs

DNA methylation and X chromosome inactivation associate EPSCs with primed pluripotency. However, we observed that EPSCs are more clonogenic and proliferate faster than PPSCs (Figure S2A), as previously reported.[35] Additionally, we and others have shown that EPSCs are able to directly convert into TSCs when switched to ASECRiAV medium,[10,25] whereas PPSCs require a priming treatment.[53–58]

Pluripotency marker analysis of 3 datasets from 3 independent groups generating EPSCs was performed. We looked at the expression of naive markers DPPA3, KLF4, KLF5, KLF17,

(C) 5mC content is expressed as the percentage of 5mC in the total pool of cytosine for the indicated cell lines. Significance levels were determined using a Kruskal Wallis test, followed by a Dunn comparison. Asterisks indicate statistical significance of the difference: $*p < 0.05$.
(D) mRNA FISH analysis for XIST, XACT, and HUWE1. Scale bar represents 10 μm.
(E) Quantification of XaXa, XaXi, and XaXe patterns. More than 100 cells were investigated for their nuclear expression for each cell line represented.

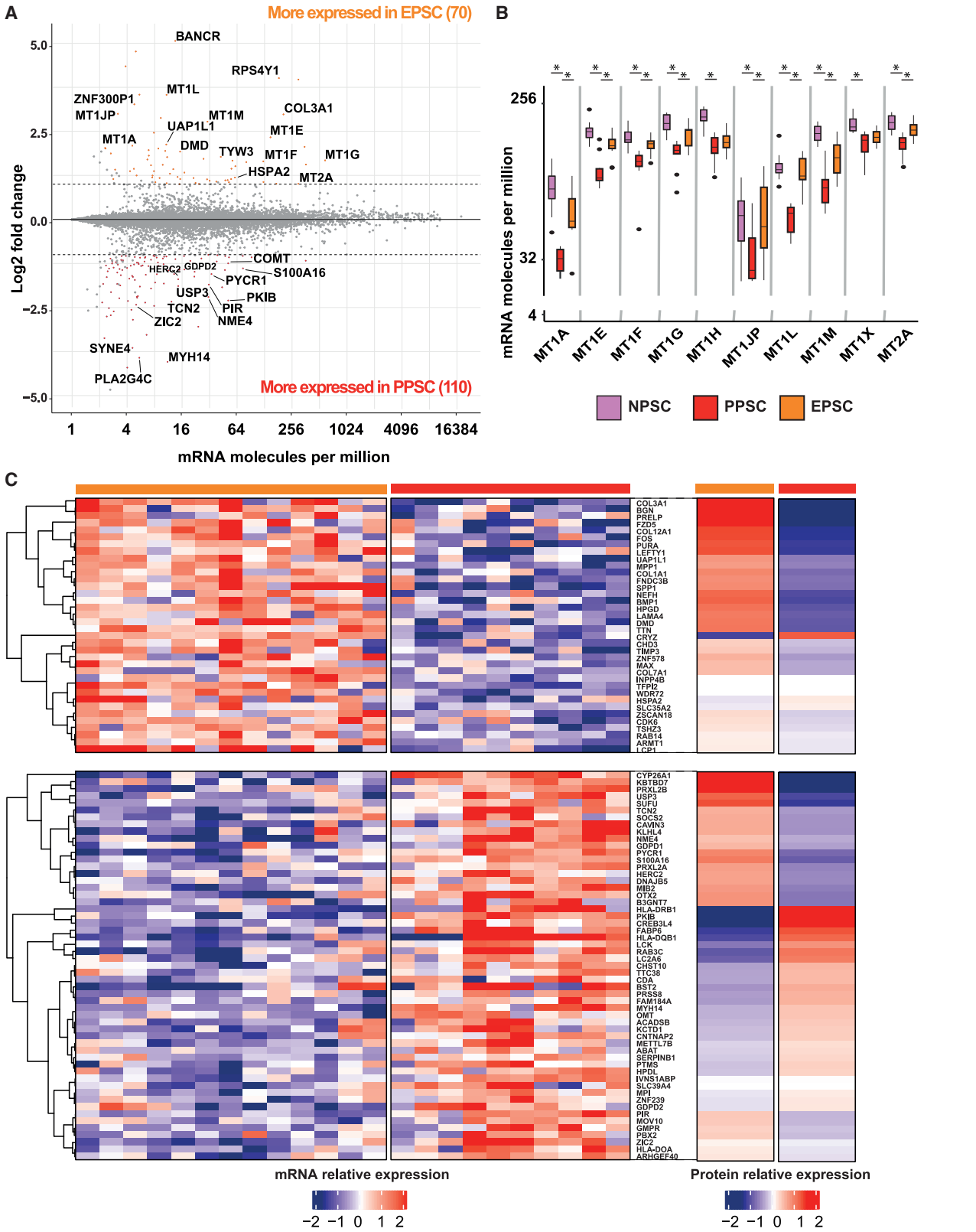

(legend on next page)

TFCP2L1, ZFP42, and ZFP57 as well as the expression of core pluripotency markers: FGF4, GDF3, NANOG, POU5F1, SALL4, SOX2, TDGF1, and UTF1. In our study, EPSCs and PPSCs express those genes similarly (Figure S2B). Of note, reanalysis of EPSC transcriptomic data from the original study by Yang et al.[35] revealed lower expression of NANOG, POU5F1, UTF1, and ZFP42 and KLF5, compared to PPSCs (from the same study, Figure S2A). We also reanalyzed Aksoy et al.'s[36] transcriptomic data. Looking at the pluripotency markers, we found that Aksoy's EPSCs express less NANOG, DPPA3, GDF3, TDGF1, ZFP42, KLF5, SALL4, and POU5F1 when compared to PPSCs (from the same study). On the other hand, NPSCs from the same study express more DPPA3, KLF5, KLF17, TFCP2L1, and ZFP57 than PPSCs and EPSCs, as expected (Figure S2D). Comparing side-by-side transcriptomic data from 3 manuscripts highlights that some markers are consistently found specific of naive (e.g., GDF3, KLF17), and it raises the question of inter-lab discrepancies in culture media formulation.

To further decipher the link between EPSCs and PPSCs, we performed differential gene expression analysis and plotted the results on an MA plot (Figure 3A). Among the 180 differentially expressed genes between our EPSCs and PPSCs, 110 are significantly downregulated genes, and less than 20 are expressed above 20 mRNA molecules per million of mRNA molecules (see STAR Methods for cutoff). Among the most differentially expressed genes, PIR and PKIB are potentially involved in nucleic acid homeostasis, and MYH14 represents an alternative myosin. Further studies are necessary to uncover the link between these pathways and the survival of EPSCs. On the other hand, 70 genes are significantly upregulated in EPSCs, and 8 of them belong to the MT1/2 family (out of 14 members detected in our analysis) (Figure 3B). Additionally, we performed a pairwise comparison of EPSCs with NPSCs and PPSCs with NPSCs, which confirmed that the most differentially expressed genes are the same in both comparisons (Figures S3A and S3B). We compared the differentially expressed genes between EPSCs and PPSCs in our dataset and in the datasets of Yang et al. and Aksoy et al. We found no differential expression of these genes in these two other datasets, showing discrepancies between cell types under similar culture conditions between laboratories (Figure S3C).

To further validate our EPSC lines at the protein level, we performed a mass spectrometry analysis on NPSCs, PPSCs, and EPSCs. 91 of the 180 differentially expressed genes were detected in the proteomics results. The expression pattern of the proteins more abundant in the EPSCs mirrors the transcriptomic expression of the associated genes (Figure 3C). However, there was more variability for the genes predominantly expressed in the PPSCs (Figure 3C). To investigate further the differences between EPSCs and PPSCs, we compared the expression levels of proteins in PPSCs, EPSCs, and NPSCs. This analysis highlighted transcription factors specifically detected in EPSCs (HES1, FOXP1, NR2F1, and SATB1) or in PPSCs (SALL2). Signaling pathway components were higher in EPSCs and NPSCs than PPSCs (FZD5, TNKS2, GDF3, PRICKLE1, and SMURF1), prompting us to investigate the role of Wnt and TGFb signaling in those cells. Finally, some surface markers stood out, such as CDH6 in EPSCs and CD74 in PPSCs (Figure S2E).

Those analyses identified specific features of EPSCs that can be followed up. Among the differentially expressed genes, the specific expression of the metallothioneins MT1A, MT1E, MT1F, MT1G, MT1JP, MT1L, MT1M, and MT2A genes in the EPSCs prompted us to perform further characterization. Metallothioneins are involved in metal metabolism[59] but also in the protection against oxidative stress.[60] As oxidative stress has been linked to metabolic activity in cancer and primary cells, we investigated metabolic-linked genes in our stem cell models.

Mitochondrial gene expression profile and metabolic activity distinguish EPSCs from PPSCs

We previously showed that electron transport chain-coding genes can distinguish naive from primed PSCs.[9] We analyzed the expression levels of the proteins composing the electron transport chain of the mitochondria. Of the 94 genes on our list, 81 were detected by mass spectrometry in all our samples. At the transcriptome level, NPSCs stand out with specific components of complex 1 (NADH dehydrogenase), while TSCs express overall low levels of electron transport chains components. However, in the proteomic analysis, EPSCs seem to be much more closely related to NPSCs. Moreover, complex 5 (ATP synthase) proteins also seem to be prevalent in TSCs (Figure 4A). Although intriguing, these data are in line with several reports showing discordance between mRNA and protein levels in several mammalian systems.[61–63]

Subsequently, to link phenotypic measurements to molecular signatures, we measured oxygen consumption rate (OCR) and extracellular acidification rate (ECAR) using MitoXpress and pHXtra kits (Figures 4B and S4A–S4D). The presentation of data as OCR vs. ECAR showed that TSCs have an oxygenation rate and an extracellular acidification rate that are two times higher than NPSCs and up to four times higher than PPSCs. Among PSCs, PPSCs have the lowest metabolic activity, and EPSCs are similar to NPSCs for this criterion, correlating with the expression of the MT1/2 expression (Figures 4B and S4A–S4E). We confirmed the higher metabolic activity of TSCs compared to NPSCs using Seahorse (Figure 4C); however, variability of measures did not allow us to determine whether EPSCs had a different

Figure 3. Refining gene signatures distinguishing EPSCs and PSCs

(A) MA plots of EPSCs and PPSCs represent the log2 fold change of gene by their mean obtained from differential gene expression analysis between two cell type annotations. Genes are colored if their adjusted p value is under 0.05 and if the fold change is greater than 2 or lower than −2.

(B) Gene expression levels of indicated genes are shown for NPSC, PPSC, and EPSC lines. The NPSC and PPSC lines are included as control. Expression levels are given as number of transcripts per million mRNA molecules. In each boxplot, the top and bottom of the box represent the third and first quartile, respectively; the band represents the median (second quartile); and error bars show the interquartile range (IQR) (lower bound: Q1 − 1.5 × IQR; upper bound: Q3 + 1.5 × IQR). p values from differential gene expression analysis were re-used for boxplots. Asterisks indicate significance compared to PPSCs: *p value < 0.05.

(C) Heatmap of relative expression of gene (left) (analyzed by DGE-seq) and associated proteins (right) (analyzed by mass spectrometry) differentially expressed between EPSC and PPSC samples.

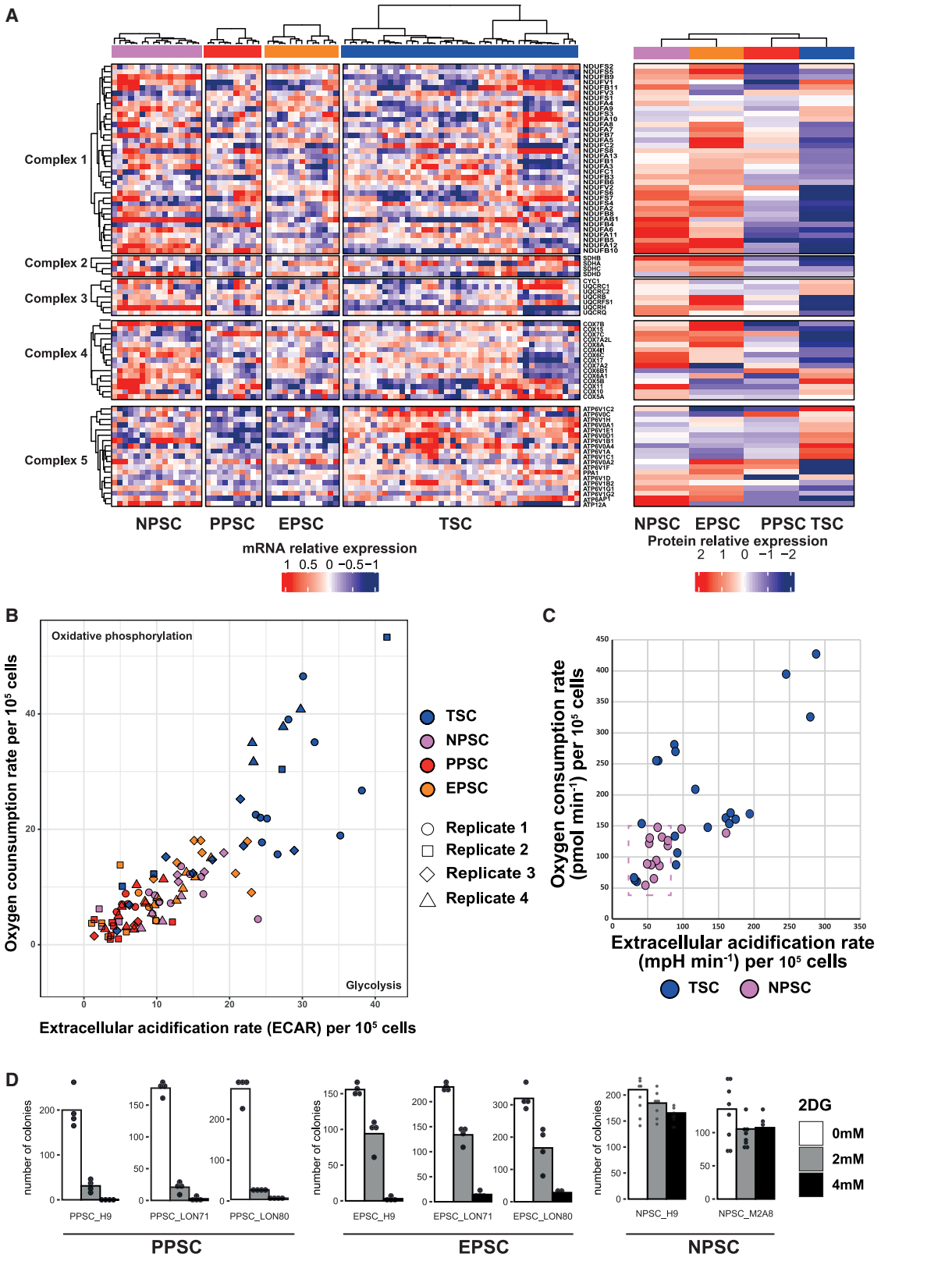

(legend on next page)

activity than NPSCs. We therefore performed a cloning assay in presence of 2 deoxy-glucose, an inhibitor of glycolysis. In those conditions, we observed that PPSCs could not survive in the presence of 2 mM 2 deoxy-glucose, EPSCs could survive in the presence of 2 mM but not 4 mM 2 deoxy-glucose, and NPSCs could survive in the presence of 4 mM 2 deoxy-glucose (Figure 4D).

Altogether, comparison of transcriptomic, proteomic, and functional assessment of metabolic activity clearly shows discrepancies based on the analysis method employed and advocates for functional tests. Nonetheless, metabolic-related readouts could clearly distinguish PPSCs, EPSCs, and NPSCs. Those results also demonstrated that additionally to higher proliferation, EPSCs have a higher metabolic activity than PPSCs.

DISCUSSION

Here, we report the comparison of TSC, EPSC, PPSC, and NPSC lines with epigenetic and functional readouts that have been previously used as hallmarks of NPSCs. Our results clarify the fact that hallmarks of pluripotency are not predictive of each other. One current issue in the human peri-implantation development field is the lack of biological reference. For example, the metabolic status of each lineage within the human peri-implantation embryo is not known yet. Considering stem cell characterization, another issue is that most hallmarks are relative. A broad array of samples needs to be assessed to have a clear view and draw conclusions. The sole comparison of 2 models is not sufficient to draw strong conclusions about fate or stage. All in all, multiplying hallmarks alleviates stage-matching biases.

Additional readouts unambiguously associated the EPSCs with a primed pluripotent fate. Nevertheless, EPSCs clearly have a higher clonogenic propensity and growth rate than PPSCs. We showed that EPSCs have a metabolic activity comparable to NPSCs, which raises a paradox in the association of hallmarks such as chimerism and trophoblastic conversion with the fate of the cells. Indeed, the ability of EPSCs to contribute to monkey and mouse chimeras,[34,35,64,65] to convert to TSCs[25,64] and to self-assemble in blastocyst-like 3D structures[32,66] questions the link between these assays with human PSCs and the conclusions we draw about fate. This discrepancy could be linked to the ''black-and-white'' way we report results, e.g., determining that a cell can or cannot contribute to chimerism or convert into TSCs. As outlined in the ISSCR standards for stem cell research, a more transparent and accurate way would be to acknowledge that indeed EPSCs can survive in animal embryos but do not invade as much as another cell state, or that EPSCs convert into TSCs after direct media transfer but at a lower rate than NPSCs. The specific behavior of EPSCs seems to uncouple survival ability to fate and developmental fate matching.[25,36] Of note, other observations could be linked to the propensity of EPSCs to differentiate directly into TSCs. First, EPSCs express high levels of the protein PCSK9, levels of which are associated with a higher proliferation rate.[67] Secondly, we detected KLF4 protein in NPSCs, TSCs, and EPSCs but not PPSCs. Since KLF4 has been identified as a key factor to go beyond PPSCs upon reprogramming,[10] it might confer enhanced plasticity to EPSCs compared to PPSCs. Nevertheless, the enhanced clonogenicity and growth rate of EPSCs offer new opportunities to understand the link between these features and pluripotency, which could open new perspectives for large-scale experiments with pluripotent cells but also could help us to explore the chimerism mechanisms and thus improve them.

The characterization of TSCs and TELCs clarifies the use of each model and provides a new reference for trophoblast models regarding their hallmarks. TSCs have an inactivated X and would correspond to cells that have low global DNA methylation levels, comparable to cytotrophoblast before 10 days post fertilization and epiblast before 8 days post fertilization.[68,69] NPSC to TSC differentiation would also be an interesting model to study the methylation waves in the embryo. Finally, defining TSC metabolic activity will help to design media that would better support post-implantation development, which needs to be improved for both human embryos and blastoids.

Altogether, systematic comparison of stem cell models is a powerful way to learn new features of peri-implantation development together with the hallmarks specific to each fate and stage. The set of hallmarks we used enabled a clearer characterization of TSCs and EPSCs along NPSCs and PPSCs. The variation between states offers the opportunity to decipher links between functions that are difficult to uncouple, such as cell cycle and fate potential. Detailed hallmarks also instruct on the relevance of each model to human development. A better understanding of human peri-implantation development using both 2D and 3D models will further deepen our understanding of early pregnancy and help to design and optimize *in vitro* fertilization techniques.

Limitations of the study

The mass spectrometry analysis was conducted with a limited number of samples (NPSC = 1, PPSC = 1, TSC = 1, EPSC = 2).

Results of RNA-seq analysis of EPSCs between different laboratories give different expression profiles. Given that we used an EPSC line from another lab (Aksoy lab), but that this line, in our hands, behaved similarly to our EPSC lines, we surmise the differences are lab-based differences in media formulation.

Figure 4. Metabolic activity of PSCs, EPSCs, NPSCs, and TSCs

(A) Heatmap of relative expression of gene (left) (analyzed by DGE-seq) and associated proteins (right) (analyzed by mass spectrometry) of electron transport chains in EPSC and PPSC samples. Genes were classified by mitochondrion complex and hierarchically clustered.

(B) Oxygen consumption rate and extracellular acidification rate of NPSCs, PPSCs, TSCs, and EPSCs were measured using MitoXpress and pHXtra kits. This figure presents 4 technical replicates.

(C) Oxygen consumption rate and extracellular acidification rate of NPSCs and TSCs were measured using a Seahorse XF apparatus. This figure presents results from 10 independent experiments.

(D) Quantification of colony numbers obtained after culture with the indicated concentrations of 2-deoxy-D-glucose (2DG).

STAR★METHODS

Detailed methods are provided in the online version of this paper and include the following:

- KEY RESOURCES TABLE
- RESOURCE AVAILABILITY
  - Lead contact
  - Materials availability
  - Data and code availability
- EXPERIMENTAL MODEL AND STUDY PARTICIPANT DETAILS
  - Cell lines
- METHOD DETAILS
  - Tissue culture - Maintenance
  - Tissue culture - TELC induction of NPSCs
  - DNA methylation
  - RNA-FISH
  - Oxygen consumption rate and extracellular acidification rate
  - Colony formation assay in 2-deoxy-D-glucose
  - 3′SRP
  - Immunostaining
  - Mass spectrometry
- QUANTIFICATION AND STATISTICAL ANALYSIS
  - Statistics
  - DGE-seq data preprocessing
  - Transcriptomic analyses
- ADDITIONAL RESOURCES

SUPPLEMENTAL INFORMATION

Supplemental information can be found online at https://doi.org/10.1016/j.celrep.2024.114232.

ACKNOWLEDGMENTS

We thank our colleagues N. Rivron, A. Camus, and P. Rugg-Gun for their insights. We thank Y. Takashima for RNA samples of ACE-TSCs. This work was supported by Theramex and ANR-22-CE91-0010. We thank the GenoBIRD, CytoCell, MicroPICell, and iPSC core facilities, all supported by IBiSA and Biogenouest, for the use of their resources and technical support. MicroPICell is a member of the national infrastructure France-Bioimaging (ANR-10-INBS-04). Bird is a member of Institut Français de Bioinformatique (IFB, ANR-11-INBS-0013). We thank P. Aubert for the access to Synergy H1 plate reader. We thank M. Schwalfenberg (Agilent) for her support for the analysis of the MitoXpress and pHXtra kits. We thank Bart Ghesquière and the Metabolomics Expertise Center (VIB-KU Leuven). Research in the Pasque laboratory was supported by the Research Foundation–Flanders (FWO; Odysseus Return Grant G0F7716N to V.P.; FWO grants G0C9320N and G0B4420N to V.P.); FWO EOS grant G0I7822N to V.P. and the KU Leuven Research Fund (C1 grant C14/21/119 to V.P.); and FWO PhD fellowships to R.N.A. (11L0722N). K.M. was supported by a fellowship from the French Medical Research Foundation (FRM SPF201809006928) and the Labex "Who Am I?" (ANR-11-LABX-0071). Research in the Rougeulle laboratory was supported by the Agence Nationale de la Recherche (ANR-14-CE10-0017 and ANR-19-CE12-0018-01), by Ligue Nationale contre le Cancer, by the European Research Council (ERC) under the European Union's Horizon 2020 research and innovation program (101020423), the LabEx 'Who Am I?' (ANR-11-LABX-0071), and the Université de Paris IdEx (ANR-18-IDEX-0001) funded by the French Government through its 'Investments for the Future' program.

AUTHOR CONTRIBUTIONS

C.O. and L.D. designed the study and wrote the manuscript with input from all authors. C.O. and E.M. performed IF analysis and cell culture experiments. S.C. and C.O. performed bioinformatics analysis. K.M., J.-F.O., and C.R. performed the FISH experiment and helped with the interpretation. C.O., E.L., and P.H. performed the 2DG experiment. I.A. provided the H9 EPSC line. V.P., G.G., and R.A. performed the methylation experiments. C.O., O.R., and C.P. performed the metabolism experiment. C.O., O.G., R.L., and C.P. performed the mass spectrometry experiment. All authors approved the final version of the manuscript.

DECLARATION OF INTERESTS

The authors declare no conflict of interest.

Received: July 11, 2023
Revised: February 2, 2024
Accepted: April 26, 2024
Published: May 17, 2024

REFERENCES

1. Rugg-Gunn, P.J., Moris, N., and Tam, P.P.L. (2023). Technical challenges of studying early human development. Development *150*, dev201797. https://doi.org/10.1242/dev.201797.
2. Thomson, J.A., Itskovitz-Eldor, J., Shapiro, S.S., Waknitz, M.A., Swiergiel, J.J., Marshall, V.S., and Jones, J.M. (1998). Embryonic Stem Cell Lines Derived from Human Blastocysts. Science *282*, 1145–1147. https://doi.org/10.1126/science.282.5391.1145.
3. Hanna, J., Cheng, A.W., Saha, K., Kim, J., Lengner, C.J., Soldner, F., Cassady, J.P., Muffat, J., Carey, B.W., and Jaenisch, R. (2010). Human embryonic stem cells with biological and epigenetic characteristics similar to those of mouse ESCs. Proc. Natl. Acad. Sci. USA *107*, 9222–9227. https://doi.org/10.1073/pnas.1004584107.
4. Takashima, Y., Guo, G., Loos, R., Nichols, J., Ficz, G., Krueger, F., Oxley, D., Santos, F., Clarke, J., Mansfield, W., et al. (2014). Resetting Transcription Factor Control Circuitry toward Ground-State Pluripotency in Human. Cell *158*, 1254–1269. https://doi.org/10.1016/j.cell.2014.08.029.
5. Chen, H., Aksoy, I., Gonnot, F., Osteil, P., Aubry, M., Hamela, C., Rognard, C., Hochard, A., Voisin, S., Fontaine, E., et al. (2015). Reinforcement of STAT3 activity reprogrammes human embryonic stem cells to naive-like pluripotency. Nat. Commun. *6*, 7095. https://doi.org/10.1038/ncomms8095.
6. Guo, G., von Meyenn, F., Santos, F., Chen, Y., Reik, W., Bertone, P., Smith, A., and Nichols, J. (2016). Naive Pluripotent Stem Cells Derived Directly from Isolated Cells of the Human Inner Cell Mass. Stem Cell Rep. *6*, 437–446. https://doi.org/10.1016/j.stemcr.2016.02.005.
7. Theunissen, T.W., Powell, B.E., Wang, H., Mitalipova, M., Faddah, D.A., Reddy, J., Fan, Z.P., Maetzel, D., Ganz, K., Shi, L., et al. (2014). Systematic Identification of Culture Conditions for Induction and Maintenance of Naive Human Pluripotency. Cell Stem Cell *15*, 471–487. https://doi.org/10.1016/j.stem.2014.07.002.
8. Takahashi, K., Tanabe, K., Ohnuki, M., Narita, M., Ichisaka, T., Tomoda, K., and Yamanaka, S. (2007). Induction of Pluripotent Stem Cells from Adult Human Fibroblasts by Defined Factors. Cell *131*, 861–872. https://doi.org/10.1016/j.cell.2007.11.019.
9. Kilens, S., Meistermann, D., Moreno, D., Chariau, C., Gaignerie, A., Reignier, A., Lelièvre, Y., Casanova, M., Vallot, C., Nedellec, S., et al. (2018). Parallel derivation of isogenic human primed and naive induced pluripotent stem cells. Nat. Commun. *9*, 360–413. https://doi.org/10.1038/s41467-017-02107-w.
10. Liu, X., Nefzger, C.M., Rossello, F.J., Chen, J., Knaupp, A.S., Firas, J., Ford, E., Pflueger, J., Paynter, J.M., Chy, H.S., et al. (2017). Comprehensive characterization of distinct states of human naive pluripotency generated by reprogramming. Nat. Methods *14*, 1055–1062. https://doi.org/10.1038/nmeth.4436.
11. Yu, J., Vodyanik, M.A., Smuga-Otto, K., Antosiewicz-Bourget, J., Frane, J.L., Tian, S., Nie, J., Jonsdottir, G.A., Ruotti, V., Stewart, R., et al. (2007). Induced Pluripotent Stem Cell Lines Derived from Human Somatic Cells. Science *318*, 1917–1920. https://doi.org/10.1126/science.1151526.

12. Gafni, O., Weinberger, L., Mansour, A.A., Manor, Y.S., Chomsky, E., Ben-Yosef, D., Kalma, Y., Viukov, S., Maza, I., Zviran, A., et al. (2013). Derivation of novel human ground state naive pluripotent stem cells. Nature *504*, 282–286. https://doi.org/10.1038/nature12745.

13. Giulitti, S., Pellegrini, M., Zorzan, I., Martini, P., Gagliano, O., Mutarelli, M., Ziller, M.J., Cacchiarelli, D., Romualdi, C., Elvassore, N., and Martello, G. (2019). Direct generation of human naive induced pluripotent stem cells from somatic cells in microfluidics. Nat. Cell Biol. *21*, 275–286. https://doi.org/10.1038/s41556-018-0254-5.

14. Yan, L., Yang, M., Guo, H., Yang, L., Wu, J., Li, R., Liu, P., Lian, Y., Zheng, X., Yan, J., et al. (2013). Single-cell RNA-Seq profiling of human preimplantation embryos and embryonic stem cells. Nat. Struct. Mol. Biol. *20*, 1131–1139. https://doi.org/10.1038/nsmb.2660.

15. Sahakyan, A., Kim, R., Chronis, C., Sabri, S., Bonora, G., Theunissen, T.W., Kuoy, E., Langerman, J., Clark, A.T., Jaenisch, R., and Plath, K. (2017). Human Naive Pluripotent Stem Cells Model X Chromosome Dampening and X Inactivation. Cell Stem Cell *20*, 87–101. https://doi.org/10.1016/j.stem.2016.10.006.

16. Vallot, C., Patrat, C., Collier, A.J., Huret, C., Casanova, M., Liyakat Ali, T.M., Tosolini, M., Frydman, N., Heard, E., Rugg-Gunn, P.J., and Rougeulle, C. (2017). XACT Noncoding RNA Competes with XIST in the Control of X Chromosome Activity during Human Early Development. Cell Stem Cell *20*, 102–111. https://doi.org/10.1016/j.stem.2016.10.014.

17. Leitch, H.G., McEwen, K.R., Turp, A., Encheva, V., Carroll, T., Grabole, N., Mansfield, W., Nashun, B., Knezovich, J.G., Smith, A., et al. (2013). Naive pluripotency is associated with global DNA hypomethylation. Nat. Struct. Mol. Biol. *20*, 311–316. https://doi.org/10.1038/nsmb.2510.

18. Guo, H., Zhu, P., Yan, L., Li, R., Hu, B., Lian, Y., Yan, J., Ren, X., Lin, S., Li, J., et al. (2014). The DNA methylation landscape of human early embryos. Nature *511*, 606–610. https://doi.org/10.1038/nature13544.

19. Smith, Z.D., Chan, M.M., Humm, K.C., Karnik, R., Mekhoubad, S., Regev, A., Eggan, K., and Meissner, A. (2014). DNA methylation dynamics of the human preimplantation embryo. Nature *511*, 611–615. https://doi.org/10.1038/nature13581.

20. Linneberg-Agerholm, M., Wong, Y.F., Romero Herrera, J.A., Monteiro, R.S., Anderson, K.G.V., and Brickman, J.M. (2019). Naïve human pluripotent stem cells respond to Wnt, Nodal and LIF signalling to produce expandable naïve extra-embryonic endoderm. Development *146*, dev180620. https://doi.org/10.1242/dev.180620.

21. Pastor, W.A., Chen, D., Liu, W., Kim, R., Sahakyan, A., Lukianchikov, A., Plath, K., Jacobsen, S.E., and Clark, A.T. (2016). Naive Human Pluripotent Cells Feature a Methylation Landscape Devoid of Blastocyst or Germline Memory. Cell Stem Cell *18*, 323–329. https://doi.org/10.1016/j.stem.2016.01.019.

22. Theunissen, T.W., Friedli, M., He, Y., Planet, E., O'Neil, R.C., Markoulaki, S., Pontis, J., Wang, H., Iouranova, A., Imbeault, M., et al. (2016). Molecular Criteria for Defining the Naive Human Pluripotent State. Cell Stem Cell *19*, 502–515. https://doi.org/10.1016/j.stem.2016.06.011.

23. De Los Angeles, A., Ferrari, F., Xi, R., Fujiwara, Y., Benvenisty, N., Deng, H., Hochedlinger, K., Jaenisch, R., Lee, S., Leitch, H.G., et al. (2015). Hallmarks of pluripotency. Nature *525*, 469–478. https://doi.org/10.1038/nature15515.

24. Wu, J., Platero-Luengo, A., Sakurai, M., Sugawara, A., Gil, M.A., Yamauchi, T., Suzuki, K., Bogliotti, Y.S., Cuello, C., Morales Valencia, M., et al. (2017). Interspecies Chimerism with Mammalian Pluripotent Stem Cells. Cell *168*, 473–486.e15. https://doi.org/10.1016/j.cell.2016.12.036.

25. Castel, G., Meistermann, D., Bretin, B., Firmin, J., Blin, J., Loubersac, S., Bruneau, A., Chevolleau, S., Kilens, S., Chariau, C., et al. (2020). Induction of Human Trophoblast Stem Cells from Somatic Cells and Pluripotent Stem Cells. Cell Rep. *33*, 108419. https://doi.org/10.1016/j.celrep.2020.108419.

26. Cinkornpumin, J.K., Kwon, S.Y., Guo, Y., Hossain, I., Sirois, J., Russett, C.S., Tseng, H.-W., Okae, H., Arima, T., Duchaine, T.F., et al. (2020). Naive Human Embryonic Stem Cells Can Give Rise to Cells with a Trophoblast-like Transcriptome and Methylome. Stem Cell Rep. *15*, 198–213. https://doi.org/10.1016/j.stemcr.2020.06.003.

27. Liu, X., Ouyang, J.F., Rossello, F.J., Tan, J.P., Davidson, K.C., Valdes, D.S., Schröder, J., Sun, Y.B.Y., Chen, J., Knaupp, A.S., et al. (2020). Reprogramming roadmap reveals route to human induced trophoblast stem cells. Nature *586*, 101–107. https://doi.org/10.1038/s41586-020-2734-6.

28. Kagawa, H., Javali, A., Khoei, H.H., Sommer, T.M., Sestini, G., Novatchkova, M., Scholte op Reimer, Y., Castel, G., Bruneau, A., Maenhoudt, N., et al. (2022). Human blastoids model blastocyst development and implantation. Nature *601*, 600–605. https://doi.org/10.1038/s41586-021-04267-8.

29. Yanagida, A., Spindlow, D., Nichols, J., Dattani, A., Smith, A., and Guo, G. (2021). Naive stem cell blastocyst model captures human embryo lineage segregation. Cell Stem Cell *28*, 1016–1022.e4. https://doi.org/10.1016/j.stem.2021.04.031.

30. Yu, L., Wei, Y., Duan, J., Schmitz, D.A., Sakurai, M., Wang, L., Wang, K., Zhao, S., Hon, G.C., and Wu, J. (2021). Blastocyst-like structures generated from human pluripotent stem cells. Nature *591*, 620–626. https://doi.org/10.1038/s41586-021-03356-y.

31. Liu, X., Tan, J.P., Schröder, J., Aberkane, A., Ouyang, J.F., Mohenska, M., Lim, S.M., Sun, Y.B.Y., Chen, J., Sun, G., et al. (2021). Modelling human blastocysts by reprogramming fibroblasts into iBlastoids. Nature *591*, 627–632. https://doi.org/10.1038/s41586-021-03372-y.

32. Sozen, B., Jorgensen, V., Weatherbee, B.A.T., Chen, S., Zhu, M., and Zernicka-Goetz, M. (2021). Reconstructing aspects of human embryogenesis with pluripotent stem cells. Nat. Commun. *12*, 5550. https://doi.org/10.1038/s41467-021-25853-4.

33. Gao, X., Nowak-Imialek, M., Chen, X., Chen, D., Herrmann, D., Ruan, D., Chen, A.C.H., Eckersley-Maslin, M.A., Ahmad, S., Lee, Y.L., et al. (2019). Establishment of porcine and human expanded potential stem cells. Nat. Cell Biol. *21*, 687–699. https://doi.org/10.1038/s41556-019-0333-2.

34. Tan, T., Wu, J., Si, C., Dai, S., Zhang, Y., Sun, N., Zhang, E., Shao, H., Si, W., Yang, P., et al. (2021). Chimeric contribution of human extended pluripotent stem cells to monkey embryos ex vivo. Cell *184*, 2020–2032.e14. https://doi.org/10.1016/j.cell.2021.03.020.

35. Yang, Y., Liu, B., Xu, J., Wang, J., Wu, J., Shi, C., Xu, Y., Dong, J., Wang, C., Lai, W., et al. (2017). Derivation of Pluripotent Stem Cells with In Vivo Embryonic and Extraembryonic Potency. Cell *169*, 243–257.e25. https://doi.org/10.1016/j.cell.2017.02.005.

36. Aksoy, I., Rognard, C., Moulin, A., Marcy, G., Masfaraud, E., Wianny, F., Cortay, V., Bellemin-Ménard, A., Doerflinger, N., Dirheimer, M., et al. (2021). Apoptosis, G1 Phase Stall, and Premature Differentiation Account for Low Chimeric Competence of Human and Rhesus Monkey Naive Pluripotent Stem Cells. Stem Cell Rep. *16*, 56–74. https://doi.org/10.1016/j.stemcr.2020.12.004.

37. Posfai, E., Schell, J.P., Janiszewski, A., Rovic, I., Murray, A., Bradshaw, B., Yamakawa, T., Pardon, T., El Bakkali, M., Talon, I., et al. (2021). Evaluating totipotency using criteria of increasing stringency. Nat. Cell Biol. *23*, 49–60. https://doi.org/10.1038/s41556-020-00609-2.

38. Okae, H., Toh, H., Sato, T., Hiura, H., Takahashi, S., Shirane, K., Kabayama, Y., Suyama, M., Sasaki, H., and Arima, T. (2018). Derivation of Human Trophoblast Stem Cells. Cell Stem Cell *22*, 50–63.e6. https://doi.org/10.1016/j.stem.2017.11.004.

39. Dong, C., Beltcheva, M., Gontarz, P., Zhang, B., Popli, P., Fischer, L.A., Khan, S.A., Park, K.M., Yoon, E.-J., Xing, X., et al. (2020). Derivation of trophoblast stem cells from naïve human pluripotent stem cells. Elife *9*, e52504. https://doi.org/10.7554/eLife.52504.

40. Io, S., Kabata, M., Iemura, Y., Semi, K., Morone, N., Minagawa, A., Wang, B., Okamoto, I., Nakamura, T., Kojima, Y., et al. (2021). Capturing human trophoblast development with naive pluripotent stem cells in vitro. Cell Stem Cell *28*, 1023–1039.e13. https://doi.org/10.1016/j.stem.2021.03.013.

41. Guo, G., Stirparo, G.G., Strawbridge, S.E., Spindlow, D., Yang, J., Clarke, J., Dattani, A., Yanagida, A., Li, M.A., Myers, S., et al. (2021). Human naive epiblast cells possess unrestricted lineage potential. Cell Stem Cell *28*, 1040–1056.e6. https://doi.org/10.1016/j.stem.2021.02.025.

42. Castel, G., and David, L. (2022). Induction of human trophoblast stem cells. Nat. Protoc. *17*, 2760–2783. https://doi.org/10.1038/s41596-022-00744-0.

43. Gerri, C., McCarthy, A., Alanis-Lobato, G., Demtschenko, A., Bruneau, A., Loubersac, S., Fogarty, N.M.E., Hampshire, D., Elder, K., Snell, P., et al. (2020). Initiation of a conserved trophectoderm program in human, cow and mouse embryos. Nature *587*, 443–447. https://doi.org/10.1038/s41586-020-2759-x.

44. Niakan, K.K., and Eggan, K. (2013). Analysis of human embryos from zygote to blastocyst reveals distinct gene expression patterns relative to the mouse. Dev. Biol. *375*, 54–64. https://doi.org/10.1016/j.ydbio.2012.12.008.

45. Meistermann, D., Bruneau, A., Loubersac, S., Reignier, A., Firmin, J., François-Campion, V., Kilens, S., Lelièvre, Y., Lammers, J., Feyeux, M., et al. (2021). Integrated pseudotime analysis of human pre-implantation embryo single-cell transcriptomes reveals the dynamics of lineage specification. Cell Stem Cell *28*, 1625–1640.e6. https://doi.org/10.1016/j.stem.2021.04.027.

46. Osnato, A., Brown, S., Krueger, C., Andrews, S., Collier, A.J., Nakanoh, S., Quiroga Londoño, M., Wesley, B.T., Muraro, D., Brumm, A.S., et al. (2021). TGFβ signalling is required to maintain pluripotency of human naïve pluripotent stem cells. Elife *10*, e67259. https://doi.org/10.7554/eLife.67259.

47. Zijlmans, D.W., Talon, I., Verhelst, S., Bendall, A., Van Nerum, K., Javali, A., Malcolm, A.A., van Knippenberg, S.S.F.A., Biggins, L., To, S.K., et al. (2022). Integrated multi-omics reveal polycomb repressive complex 2 restricts human trophoblast induction. Nat. Cell Biol. *24*, 858–871. https://doi.org/10.1038/s41556-022-00932-w.

48. Girard, O., Lavigne, R., Chevolleau, S., Onfray, C., Com, E., Schmit, P.-O., Chapelle, M., Fréour, T., Lane, L., David, L., and Pineau, C. (2023). Naive Pluripotent and Trophoblastic Stem Cell Lines as a Model for Detecting Missing Proteins in the Context of the Chromosome-Centric Human Proteome Project. J. Proteome Res. *22*, 1148–1158. https://doi.org/10.1021/acs.jproteome.2c00496.

49. Vallot, C., Ouimette, J.F., Makhlouf, M., Féraud, O., Pontis, J., Côme, J., Martinat, C., Bennaceur-Griscelli, A., Lalande, M., and Rougeulle, C. (2015). Erosion of X Chromosome Inactivation in Human Pluripotent Cells Initiates with XACT Coating and Depends on a Specific Heterochromatin Landscape. Cell Stem Cell *16*, 533–546. https://doi.org/10.1016/j.stem.2015.03.016.

50. Sahakyan, A., Kim, R., Chronis, C., Sabri, S., Bonora, G., Theunissen, T.W., Kuoy, E., Langerman, J., Clark, A.T., Jaenisch, R., and Plath, K. (2017). Human Naive Pluripotent Stem Cells Model X Chromosome Dampening and X Inactivation. Cell Stem Cell *20*, 87–101. https://doi.org/10.1016/j.stem.2016.10.006.

51. Cloutier, M., Kumar, S., Buttigieg, E., Keller, L., Lee, B., Williams, A., Mojica-Perez, S., Erliandri, I., Rocha, A.M.D., Cadigan, K., Smith, G.D., and Kalantry, S. (2022). Preventing erosion of X-chromosome inactivation in human embryonic stem cells. Nat. Commun. *13*, 2516. https://doi.org/10.1038/s41467-022-30259-x.

52. Karvas, R.M., Khan, S.A., Verma, S., Yin, Y., Kulkarni, D., Dong, C., Park, K.-M., Chew, B., Sane, E., and Fischer, L.A. (2022). Stem-cell-derived Trophoblast Organoids Model Human Placental Development and Susceptibility to Emerging Pathogens. Cell Stem Cell *29*, 810–825.e8.

53. Mischler, A., Karakis, V., Mahinthakumar, J., Carberry, C.K., San Miguel, A., Rager, J.E., Fry, R.C., and Rao, B.M. (2021). Two distinct trophectoderm lineage stem cells from human pluripotent stem cells. J. Biol. Chem. *296*, 100386. https://doi.org/10.1016/j.jbc.2021.100386.

54. Wei, Y., Wang, T., Ma, L., Zhang, Y., Zhao, Y., Lye, K., Xiao, L., Chen, C., Wang, Z., Ma, Y., Zhou, X., Sun, F., Li, W., Dunk, C., Li, S., Nagy, A., Yu, Y., Pan, G., Lye, S.J., and Shan, Y. (2021). Efficient derivation of human trophoblast stem cells from primed pluripotent stem cells. Sci Adv. *7*, eabf4416. https://doi.org/10.1126/sciadv. abf4416.

55. Jang, Y.J., Kim, M., Lee, B.K., and Kim, J. (2022). Induction of human trophoblast stem-like cells from primed pluripotent stem cells. Proc. Natl. Acad. Sci. USA *119*, e2115709119. https://doi.org/10.1073/pnas.2115709119.

56. Soncin, F., Morey, R., Bui, T., Requena, D.F., Cheung, V.C., Kallol, S., Kittle, R., Jackson, M.G., Farah, O., Chousal, J., et al. (2022). Derivation of functional trophoblast stem cells from primed human pluripotent stem cells. Stem Cell Rep. *17*, 1303–1317. https://doi.org/10.1016/j.stemcr.2022.04.013.

57. Viukov, S., Shani, T., Bayerl, J., Aguilera-Castrejon, A., Oldak, B., Sheban, D., Tarazi, S., Stelzer, Y., Hanna, J.H., and Novershtern, N. (2022). Human primed and naïve PSCs are both able to differentiate into trophoblast stem cells. Stem Cell Rep. *17*, 2484–2500. https://doi.org/10.1016/j.stemcr.2022.09.008.

58. Zorzan, I., Betto, R.M., Rossignoli, G., Arboit, M., Drusin, A., Corridori, C., Martini, P., and Martello, G. (2023). Chemical conversion of human conventional PSCs to TSCs following transient naive gene activation. EMBO Rep. *24*, e55235. https://doi.org/10.15252/embr.202255235.

59. Balogh, E., Veale, D.J., McGarry, T., Orr, C., Szekanecz, Z., Ng, C.-T., Fearon, U., and Biniecka, M. (2018). Oxidative stress impairs energy metabolism in primary cells and synovial tissue of patients with rheumatoid arthritis. Arthritis Res. Ther. *20*, 95. https://doi.org/10.1186/s13075-018-1592-1.

60. Kumari, M.V., Hiramatsu, M., and Ebadi, M. (1998). Free radical scavenging actions of metallothionein isoforms I and II. Free Radic. Res. *29*, 93–101. https://doi.org/10.1080/10715769800300111.

61. Edfors, F., Danielsson, F., Hallström, B.M., Käll, L., Lundberg, E., Pontén, F., Forsström, B., and Uhlén, M. (2016). Gene-specific correlation of RNA and protein levels in human cells and tissues. Mol. Syst. Biol. *12*, 883. https://doi.org/10.15252/msb.20167144.

62. Schwanhäusser, B., Busse, D., Li, N., Dittmar, G., Schuchhardt, J., Wolf, J., Chen, W., and Selbach, M. (2011). Global quantification of mammalian gene expression control. Nature *473*, 337–342. https://doi.org/10.1038/nature10098.

63. van den Berg, P.R., Bérenger-Currias, N.M.L.P., Budnik, B., Slavov, N., and Semrau, S. (2023). Integration of a multi-omics stem cell differentiation dataset using a dynamical model. PLoS Genet. *19*, e1010744. https://doi.org/10.1371/journal.pgen.1010744.

64. Liu, B., Chen, S., Xu, Y., Lyu, Y., Wang, J., Du, Y., Sun, Y., Liu, H., Zhou, H., Lai, W., et al. (2021). Chemically defined and xeno-free culture condition for human extended pluripotent stem cells. Nat. Commun. *12*, 3017. https://doi.org/10.1038/s41467-021-23320-8.

65. Zheng, R., Geng, T., Wu, D.-Y., Zhang, T., He, H.-N., Du, H.-N., Zhang, D., Miao, Y.-L., and Jiang, W. (2021). Derivation of feeder-free human extended pluripotent stem cells. Stem Cell Rep. *16*, 2410–2414. https://doi.org/10.1016/j.stemcr.2021.07.019.

66. Fan, Y., Min, Z., Alsolami, S., Ma, Z., Zhang, E., Chen, W., Zhong, K., Pei, W., Kang, X., Zhang, P., et al. (2021). Generation of human blastocyst-like structures from pluripotent stem cells. Cell Discov. *7*, 81. https://doi.org/10.1038/s41421-021-00316-8.

67. Roudaut, M., Idriss, S., Caillaud, A., Girardeau, A., Rimbert, A., Champon, B., David, A., Lévêque, A., Arnaud, L., Pichelin, M., et al. (2021). PCSK9 regulates the NODAL signaling pathway and cellular proliferation in hiPSCs. Stem Cell Rep. *16*, 2958–2972. https://doi.org/10.1016/j.stemcr.2021.10.004.

68. Zhou, F., Wang, R., Yuan, P., Ren, Y., Mao, Y., Li, R., Lian, Y., Li, J., Wen, L., Yan, L., et al. (2019). Reconstituting the transcriptome and DNA methylome landscapes of human implantation. Nature *572*, 660–664. https://doi.org/10.1038/s41586-019-1500-0.

69. Santos, F., Hyslop, L., Stojkovic, P., Leary, C., Murdoch, A., Reik, W., Stojkovic, M., Herbert, M., and Dean, W. (2010). Evaluation of epigenetic

marks in human embryos derived from IVF and ICSI. Hum. Reprod. *25*, 2387–2395. https://doi.org/10.1093/humrep/deq151.

70. Bredenkamp, N., Yang, J., Clarke, J., Stirparo, G.G., von Meyenn, F., Dietmann, S., Baker, D., Drummond, R., Ren, Y., Li, D., et al. (2019). Wnt Inhibition Facilitates RNA-Mediated Reprogramming of Human Somatic Cells to Naive Pluripotency. Stem Cell Rep. *13*, 1083–1098. https://doi.org/10.1016/j.stemcr.2019.10.009.

71. Charpentier, E., Cornec, M., Dumont, S., Meistermann, D., Bordron, P., David, L., Redon, R., Bonnaud, S., and Bihouée, A. (2021). 3' RNA Sequencing for Robust and Low-Cost Gene Expression Profiling (Protocol Exchange. https://doi.org/10.21203/rs.3.pex-1336/v1.

72. Banliat, C., Tsikis, G., Labas, V., Teixeira-Gomes, A.-P., Com, E., Lavigne, R., Pineau, C., Guyonnet, B., Mermillod, P., and Saint-Dizier, M. (2020). Identification of 56 Proteins Involved in Embryo–Maternal Interactions in the Bovine Oviduct. Int. J. Mol. Sci. *21*, 466. https://doi.org/10.3390/ijms21020466.

73. Bruderer, R., Bernhardt, O.M., Gandhi, T., Xuan, Y., Sondermann, J., Schmidt, M., Gomez-Varela, D., and Reiter, L. (2017). Optimization of Experimental Parameters in Data-Independent Mass Spectrometry Significantly Increases Depth and Reproducibility of Results. Mol. Cell. Proteomics *16*, 2296–2309. https://doi.org/10.1074/mcp.RA117.000314.

74. Deutsch, E.W., Csordas, A., Sun, Z., Jarnuczak, A., Perez-Riverol, Y., Ternent, T., Campbell, D.S., Bernal-Llinares, M., Okuda, S., Kawano, S., et al. (2017). The ProteomeXchange consortium in 2017: supporting the cultural change in proteomics public data deposition. Nucleic Acids Res. *45*, D1100–D1106. https://doi.org/10.1093/nar/gkw936.

75. Vizcaíno, J.A., Côté, R.G., Csordas, A., Dianes, J.A., Fabregat, A., Foster, J.M., Griss, J., Alpi, E., Birim, M., Contell, J., et al. (2013). The Proteomics Identifications (PRIDE) database and associated tools: status in 2013. Nucleic Acids Res. *41*, D1063–D1069. https://doi.org/10.1093/nar/gks1262.

76. Leek, J.T., Evan Johnson, W., Parker, H.S., Fertig, E.J., Jaffe, A.E., Zhang, Y., Storey, J.D., and Torres, L.C. (2022). sva: Surrogate Variable Analysis. Version 3.46.0 (Bioconductor version: Release (3.16)). https://doi.org/10.18129/B9.bioc.sva.

77. Gu, Z., Eils, R., and Schlesner, M. (2016). Complex heatmaps reveal patterns and correlations in multidimensional genomic data. Bioinformatics *32*, 2847–2849. https://doi.org/10.1093/bioinformatics/btw313.

78. Gu, Z. (2022). Complex heatmap visualization. iMeta *1*, e43. https://doi.org/10.1002/imt2.43.

79. Love, M.I., Huber, W., and Anders, S. (2014). Moderated estimation of fold change and dispersion for RNA-seq data with DESeq2. Genome Biol. *15*, 550. https://doi.org/10.1186/s13059-014-0550-8.

80. Zhu, A., Ibrahim, J.G., and Love, M.I. (2019). Heavy-tailed prior distributions for sequence count data: removing the noise and preserving large differences. Bioinformatics *35*, 2084–2092. https://doi.org/10.1093/bioinformatics/bty895.

STAR★METHODS

KEY RESOURCES TABLE

REAGENT or RESOURCE	SOURCE	IDENTIFIER
Antibodies		
GATA2	Sigma-Aldrich	WH0002624M1
GATA3	R&D	AF2605
NR2F2	Abcam	ab211776
CDX2	Cell Signaling	Cat# D11D10
NANOG	R&D systems	Cat# AF1997; RRID:AB_355097
NANOG	Thermofisher	Cat# PA1-097; RRID:AB_2539867
Antibodies are also listed in Table S1.		
Chemicals, peptides, and recombinant proteins		
Y27632 (ROCK inhibitor)	Axon Medchem	1683
Insulin-Transferrin-Selenium-Ethanolamine supplement (ITS-X)	GIBCO	51500–056
L-ascorbic acid	Sigma-Aldrich	A7506
hEGF	Miltenyi Biotec	130-097-751
CHIR99021	Axon Medchem	1386
A83-01	Axon Medchem	1421
SB431542	Axon Medchem	1661
valproic acid	Sigma-Aldrich	P4543
PD0325901	Axon Medchem	1408
mLIF	Miltenyi Biotec	130-095-779
Gö6983	Axon Medchem	2466
XAV	Axon Medchem	1527
N2 supplement	GIBCO	17502048
B27 supplement	GIBCO	17504–001
B27 supplement minus vitamin A	GIBCO	12587010
human LIF	Miltenyi Biotec	130-108-156
(S)-(+)-Dimethindene maleate	Tocris	1425
Minocycline hydrochloride	Tocris	3268
IWR-*endo*-1	Axon Medchem	2510
DMEM-F12	GIBCO	31330095
GlutaMAX	GIBCO	35050–38
Fetal bovine serum	Hyclone	SV30160.03
Sodium pyruvate	Life Technologies	11360070
MEM NEAA	GIBCO	11140–035
Bovine Serum Albumin (BSA)	Sigma-Aldrich	A3059
Neurobasal	GIBCO	21103049
KSR	GIBCO	10828028
2-mercaptoethanol	GIBCO	31350–010
Penicillin-streptomycin	GIBCO	15140–122
Mitomycin C	Sigma-Aldrich	M4287
mTeSR1	StemCell Technologies	85851
Matrigel	Corning	354277
Geltrex	GIBCO	A1569601
TrypLE Express	GIBCO	12605–010

(*Continued on next page*)

Continued

REAGENT or RESOURCE	SOURCE	IDENTIFIER
pH-Xtra Reagent	Agilent	PH-200-4
MitoXpress Xtra Reageat	Agilent	MX-200-4
Vectashield	Vector laboratories	H-1000-10
DNase	Roche	04716728001
DNAse buffer	Roche	04716728001
Polymerase I	Promega	M205B
green dUTP	Abbot Molecular	02N32-050
red dUTP	Abbot Molecular	02N34-050
orange (Cy3) dUTP	Abbot Molecular	02N33-050
SIGMA FASTTM BCIP®/NBT kit	SIGMA	B5655-25TAB
Acetonitrile, Optima™ LC/MS Grade	Fisher Chemical™	A955-212
Formic acid, 99.0%, Optima™ LC/MS Grade	Fisher Chemical™	A11710X1-AMP
2 deoxy glucose	SIGMA	D6134
Antimycin A	SIGMA	A8674
Rotenone	SIGMA	557368
Critical commercial assays		
iST kit	PreOmics	P.O.00001
iST-Fractionation Add-on	PreOmics	P.0.00100
Bicinchoninic Acid Kit for Denaturation Determination	Sigma-Aldrich	BCA-1
Pierce™ Quantitative Peptide Assays & Standards	Thermo Scientific™	23275
RNeasy-Mini Kit	Qiagen	Cat. No./ID: 74104
Large Construct kit	Qiagen	Cat. No./ID: 12462
QIAamp DNA Mini Kit	Qiagen	Cat. No./ID: 51304
Deposited data		
3'SRP data	ENA	PRJEB63637
DIA Mass spectrometry data	ProteomeXchange Consortium	PXD043712
Experimental models: Cell lines		
All cell lines are detailed in Table S3A		
Recombinant DNA		
XIST	10 kb Exon 5–6, gift from Dr. Edith Heard, EMBL, Germany	
XACT	BACPAC	RP11-35D3
HUWE1	BACPAC	RP11-42M11
Software and algorithms		
Volocity	Quorum technologies	V6.3
Fiji	ImageJ	V1.53c
R	Bioconductor	v 4.0.3
Other		
HeLa Protein Digest Standard - Pierce™	Thermo Scientific™	PI88329
E. Coli 2.7mg	Biorad	163–2110

RESOURCE AVAILABILITY

Lead contact

Further information and requests for resources and reagents should be directed to and will be fulfilled by the lead contact, Laurent David (laurent.david@univ-nantes.fr)

Materials availability

This study did not generate new unique reagents. Cell lines used in this study are available, pending MTA and regulatory authorizations.

Data and code availability

- Data have been deposited on ENA (PRJEB63637).
- scRNAseq alignment pipeline: https://gitlab.univ-nantes.fr/E114424Z/SingleCell_Align.
- Data preprocessing script and analysis scripts are available at the following link: https://gitlab.univ-nantes.fr/E198672Y/onfray-et-al-2022.
- Any additional information required to reanalyze the data reported in this work paper is available from the lead contact upon request.

EXPERIMENTAL MODEL AND STUDY PARTICIPANT DETAILS

Cell lines

All cell lines are detailed in Table S3A. In brief, induced naive, primed or extended PSC lines were reprogrammed from fibroblasts: L71 from a 51-year-old healthy man; L80 from a 57-year-old healthy woman; MIPS220 from a healthy female in her 30's.[9,25] human embryonic stem cells H9 (WA09) were imported and used with authorization RE17-007R from the French oversight committee, Agence de la Biomédecine. H9-EPSC were generated by I. Aksoy. Naive H9 were generated in C. Rougeulle lab (Vallot et al.). TSCs lines we used were generated by Okae et al., or Castel et al.

For TELC differentiation experiments we used M2A8 NPSCs line from Kilens et al.

METHOD DETAILS

Tissue culture - Maintenance

All cell lines were cultured at 37 °C, either under hypoxic (5% O2, 5% CO2) or normoxic conditions (20% O2, 5% CO2) as indicated. Culture medium was daily replaced. 10 μM Y27632 (Axon Medchem) was added to the culture medium upon single-cell seeding of all human stem cells. PXX indicates passage number. All cell lines were tested negative for mycoplasma using the MycoAlert kit (LONZA, LT07-318).

Mouse embryonic fibroblasts (MEFs) were prepared from E13.5 pups that were decapitated, eviscerated, dissociated with 0.25% trypsin, 0.1% EDTA and plated in MEF medium [DMEM high glucose (Thermo Scientific), Glutamax 1:100 (GIBCO), 0.5% of penicillin–streptomycin (Life Technologies)] on 0.1% gelatin-coated plates. MEFs were mitotically inactivated using 0.01 mg/ml mitomycin C (Sigma-Aldrich) to be used as feeder cells. MEF isolation was performed in compliance with the French law and under supervision of the UTE animal core facility, Nantes Université.

TSCs were cultured on MEF feeder cells in ASECRiAV medium[38] [DMEM/F12 (GIBCO) supplemented with 0.1mM 2-mercaptoethanol (GIBCO), 0.2% FBS, 0.5% penicillin-streptomycin, 0.3% Bovine Serum Albumin (BSA, Sigma-Aldrich), 1% Insulin-Transferrin-Selenium-Ethanolamine supplement (ITS-X, GIBCO), 1.5 mg/mL L-ascorbic acid (Sigma-Aldrich), 50 ng/mL hEGF (Miltenyi Biotec), 2 μM CHIR99021 (Axon Medchem), 0.5 μM A83-01 (Tocris), 1 μM SB431542 (Tocris), 0.8 mM valproic acid (Sigma-Aldrich) and 5 μM Y27632]. TSCs could be passaged with TrypLE (5–10 min, 37°C, Life Technologies) every 4 to 5 days at a cell density between 1.04*10^4 and 2.08 *10^4 cells per cm^2. TSCs were routinely cultured at 37°C in hypoxic conditions.

NPSCs were cultured on MEF feeder cells in t2iLGöY medium[4] [DMEM/F12 supplemented with 1% N2 (GIBCO), 1% B27 (GIBCO), 1% non-essential amino acids, 1% GlutaMAX (GIBCO), 0.1 mM 2-mercaptoethanol, 50 μg/mL BSA, 0.5% penicillin–streptomycin, 1 μM CHIR99021, 1 μM PD0325901 (Axon Medchem), 20 ng/mL mLIF (Miltenyi Biotec), 5 μM Gö6983 (Axon Medchem) and 10 μM Y27632] or PXGL[70] medium [47.5% Neurobasal medium (GIBCO) and 47.5% DMEM/F12 (GIBCO) supplemented with 1mM N2 (GIBCO), 2mM B27 (GIBCO), 1mM GlutaMAX (GIBCO), 1mM non-essential amino acids (GIBCO), 0.33% BSA, 1mM sodium pyruvate (GIBCO), 0.1% 2-mercaptoethanol (GIBCO), 0.5% penicillin-streptomycin, 1μM PD0325901 (Axon Medchem), 2μM XAV939 (Axon medchem), 2 μM Gö6983 (Axon medchem), 10 ng/mL hLif (Peprotech), 10μM Y27632 (Axon Medchem)]. NPSCs were passaged every 4 to 5 days at a cell density of 2.08 *10^4 cells per cm^2 using TrypLE (5 min, 37°C, Life Technologies). NPSCs were routinely cultured at 37 °C in hypoxic conditions.

EPSCs were cultured on MEF feeder cells in LCDM medium[35] [48% DMEM/F12 and 48% Neurobasal (GIBCO) supplemented with 0.5% N2 supplement, 1% B27 supplement minus vitamin A (GIBCO), 1% non-essential amino acids, 0.1 mM 2-mercaptoethanol, 0.5% penicillin-streptomycin, 5% knockout serum replacement (KSR, GIBCO), 10 ng/mL human LIF (Miltenyi Biotec), 1μM CHIR99021, 2 μM (S)-(+)-Dimethindene maleate (Tocris) and 2 μM Minocycline hydrochloride (Tocris), 1 μM IWR-*endo*-1 (Miltenyi Biotec) and 2 μM Y-27632]. EPSCs were passaged every 4 to 5 days at a 1:20 to 1:40 split ratio using TrypLE (5 min, 37°C, Life Technologies). EPSCs were routinely cultured at 37°C in normoxic conditions.

Primed PSCs were cultured on matrigel 0.1% in mTeSR1 medium (StemCell technologies). Colonies were manually divided every 5 to 6 days for passage, following 3min in gentle cell dissociation reagent (Miltenyi Biotec) and seeded as small clumps in a new MW6 well. Primed PSCs were routinely cultured at 37°C in normoxic conditions.

Tissue culture - TELC induction of NPSCs

Differentiation of NPSCs into trophectoderm-like cells was performed according to Guo et al. protocol[41]: NPSCs are passaged with TrypLE (5 min, 37°C, Life Technologies) and plated in 24-well plates on Geltrex (0.5mL per cm2, Gibco) at 1:1 ratio. Before plating, a

MEFs exclusion is performed on a 0.1% gelatine (Sigma) coated 6-well plate for 30 min in PXGL + Y27632. At day −1, the cells are cultured in PXGL + Y27632. From day 0, the medium is changed into N2B27 supplemented with 1μM PD0325901 (Axon Medchem) and 1μM A83-01 (Tocris). Cells are cultured for up to 5 days at 37°C in hypoxic conditions.

DNA methylation

We tested DNA methylation in three batches composed of, for batch 1: 3 technical replicates of NPSCs (M2A8), 2 technical replicates of EPSCs (E80), 3 biological replicates with each 2 technical replicates for TSC (CT30, AV03, AV23), 3 technical replicates of PPSCs (MIPS220). For batch 2: 2 technical replicates of NPSCs (M2A8), 1 technical replicate of EPSCs (E80), 3 biological replicates with each 2 technical replicates for TSC (CT30, AV03, AV23), 1 technical replicate of PPSCs (MIPS220). For batch 3: 2 technical replicates of NPSCs from,[47] 3 biological replicates of EPSCs (E80, E71, H9), 1 technical replicate for TSC (AV23), 2 biological replicates of PPSCs (H9, MIPS220). For mass spectrometry analysis of DNA methylation, DNA was extracted using the genomic DNA columns (Qiagen). 1 μg of genomic DNA was analyzed using liquid chromatography triple-quadrupole mass spectrometry (KU Leuven Metabolomics Core). The concentration (μM) of Cytosine (unmodified), 5mC and 5-hydroxymethyl-cytosine (5hmC) were obtained using standard curves of known C, 5mC and 5hmC amounts. The percentage of 5mC or 5hmC in DNA was obtained by calculating the ratio of 5mC or 5hmC to the total pool of C.

RNA-FISH

RNA-FISH was performed as previously described (Kilens et al., 2018). Briefly, cells were fixed between 24h and 50 h post seeding in 3% paraformaldehyde for 10 min at room temperature. Cells were permeabilized in CSK buffer supplemented with 1 mM EGTA, 0.5% Triton and VRC (200μM) for 5 min on ice. After 3 washes in 70% EtOH, cells were dehydrated in 90% and 100% EtOH and incubated overnight with probes at 37 °C. After three 50% formaldehyde/2× SSC washes and three 2× SSC washes at 42 °C for 4 min, coverslips were mounted in Vectashield plus DAPI. SpectrumGreen or SpectrumRed-labeled probes (Vysis) were generated by nick translation for human XIST (10 kb Exon 5–6, gift from Dr. Edith Heard, EMBL, Germany), XACT (RP11-35D3, BACPAC) and HUWE1 (RP11-42M11, BACPAC Resource). Probes preparation: RNA-FISH probes were obtained after Nick translation of fosmids/BAC constructs purified using the Large Construct kit (Qiagen): 1ug of purified DNA was labeled using nick translation using for a final volume of 50uL: 1μg DNA, 0.04U of Dnase (Roche), Polymerase I (Promega, M205B), 0.01M DTT, 0.02mM dATP/dCTP/dGTP, 0.01mM dTTP, 0.1mM dUTP (green dUTP 02N32-050 (Abbot Molecular); red dUTP 02N34-050 (Abbot Molecular); orange (Cy3) dUTP 02N33-050 (Abbot Molecular) in DNAse buffer (Roche, 04716728001). Reactions are incubated for 3 h at 15°C. Images were acquired on an inverted Nikon A1 confocal microscope, according to the Shannon–Nyquist sampling rate. mRNA expression of XIST, XACT and HUWE1 are manually counted in more than 100 cells per cell line: 100 cells are randomly chosen for each sample. The number of dots per cell for each channel is quantified. Dots are considered when present on more than 2 z-plans. Dots on different channels are considered on the same chromosome only when less than 2μm from each other. Cells with a pattern that appears to show more than two distinct dots in at least one channel are considered as ‘‘chromosomal abnormalities’’. Cells with a pattern without HUWE1 are pooled in ‘‘Others’’. Cells with no visible dots are pooled in ‘‘Nothing’’. At least two biological replicates are done for each cell line (Table S3A).

Oxygen consumption rate and extracellular acidification rate

To assess metabolic activity of the human peri-implantation cellular models, we measured the oxygen consumption rate and the extracellular acidification rate.

Oxygen consumption rate was measured by measuring fluorescence signal coupled with oxygen concentration, using MitoXpress kit (Agilent). Extracellular acidification rate was measured by measuring fluorescence signal coupled with pH variation, using pHXtra kit (Agilent). Both analyses were performed conjointly. Slopes of variation of fluorescence over 30min were extracted for the analysis. Synergy H1 plate reader, with dual read TR-F was used for the measures.

The experiment was conducted 4 times, on 4 technical replicates, and included 2 biological replicates for EPSCs (E80, E71), 3 for TSCs (CT30, AV03, AV23), with 1 biological replicate of NPSCs (M2A8) and 3 biological replicates of PPSCs (LON80, LON71, MIPS220) as controls.

Before seeding, black sides clear bottom plates were pretreated for 20min with 2 μg/mL of Cell-Tak Cell and tissue adhesive (Corning).

NPSCs, PPSCs, EPSCs and TSCs were dissociated using TrypLE for 5 min at 37°C. NPSCs, EPSCs and TSCs were incubated on gelatin (0.1%) for 30 min at 37 °C to remove feeder cells. Cells were resuspended in DMEM (Sigma Aldrich) supplemented with 10 mM glucose, 2 mM glutamine, 2 mM pyruvate and pH was adjusted to 7.4 using NaOH.

A cell seeding density titration experiment was performed before the first experiment to determine the optimal quantity of cells for the experiments. Respectively, NPSCs, PPSCs, EPSCs and TSCs were seeded at 0.5625*10^6, 1.125*10^6, 0.5156*10^6 and 0.5156 *10^6 cells per cm^2.

To control that measurements were performed appropriately, we included controls to check the maximal respiratory capacity (FCCP, 0.75 μM), inhibition of oxidative phosphorylation (Antimycin-A, 2 μM and Rotenone, 1 μM), and inhibition of glycolysis (2DG, 50mM). Those controls validated that our measurements were within detection limits and metabolic capacity of the cells (data not shown).

Colony formation assay in 2-deoxy-D-glucose

NPSCs, EPSCs or PPSCs were seeded at 2000 cells per well in a 12-well plate, on top of feeders, in their respective media in addition to 10 μM Y27632. From day 1 after seeding onwards, 2 mM or 4 mM of 2-deoxy-D-glucose were supplemented in the culture medium. Cells were fixed between day 4 and day 6 post seeding and stained for alkaline phosphatase using the SIGMA FAST BCIP/NBT kit (Sigma). Images were acquired using the Cellomics ArrayscanVTI (Thermo Fisher) at a 5× magnification. Colonies were counted manually.

3′SRP

Total RNA molecules were extracted from cells with RNeasy-Mini Kits (Qiagen). Protocol of 3′ SRP RNA sequencing was performed as previously described in.[71] Libraries were then sequenced on a NovaSeq 6000 (Illumina). Data were aligned along the human genome reference (hg19) and a count matrix was generated by counting sample specific UMI associated with genes for each sample. Samples with less than 200 000 UMI and less than 5000 genes expressed were excluded of the analysis. Then, a batch correction between samples of different experiments was applied. A Principal Component Analysis (PCA) was performed in order to visualized samples repartition by reducing the number of dimensions. Correlation between samples were assessed with Pearson's linear correlation heatmaps. Higher correlations are marked in yellow and lower correlations are in red. Differentially expressed genes between conditions were calculated using R package Deseq2 (Bioconductor) by first applying a variance stabilizing transformation (vst). Genes with adjusted *p*-value inferior to 0.05 and with a fold change superior to 2 or inferior to −2 were considered as differentially expressed genes. Gene expressions were visualized with heatmaps that were generated by center genes expression. Finally, pathways analysis was performed: R package "Fgsea" and databases such as Kegg, Reactome and Gene Ontology were used to identify significantly enriched or depleted groups of genes in each condition.

Of note, 3'SRP, the RNAseq method we are using, allows us to correlate the expression level with the likeness of protein to be expressed.[48] Indeed, up to 70.45% genes are identified by MS/MS analysis when their expression level is above 20 mRNA molecules per million of mRNA molecules.

Immunostaining

For immunofluorescence (IF) analysis, cells were fixed at room temperature using 4% paraformaldehyde for 15 min. Samples were then permeabilized for 60 min at room temperature with IF buffer [phosphate-buffered saline (PBS), 0.2% Triton, 10% FBS], which also served as a blocking solution. Samples were incubated with primary antibodies overnight at 4 °C. The following antibodies were used: anti-GATA3 (1:300, R&D AF2605), anti-NR2F2 (1:300, Abcam ab211776), anti-CDX2 (1:300, Abcam ab157524). Incubation with secondary antibodies was performed for 2 h at room temperature along with 4′,6-diamidino-2-phenylindole (DAPI) nuclei staining. Confocal immunofluorescence images were acquired with A1-SIM Nikon confocal microscope. Optical sections of 0.5–1 μm-thick were collected. Images were processed using Volocity visualization software and Fiji software (http://fiji.sc).

Mass spectrometry

Cell culture for mass spectrometry

For all samples (except EPSCs) we performed 2 types of sample preparation: Lysis after TrypIE dissociation or Lysis without TrypIE dissociation.

NPSCs: 1 day prior lysis (4–5 days after seeding), NPSCs, were dissociated using TrypLE for 5 min at 37°C. NPSCs were incubated on gelatin (0.1%) for 1h at 37 °C to remove feeder cells. NPSCs were plated overnight respectively on a 0.1% geltrex coated plate (1/1 ratio). The next day, cells were rinsed with PBS−/− before being lysed using the iST kit (PreOmics GmbH, Planegg, Germany) following the manufacturer's instructions.

The lysis day, another well of NPSCs was dissociated using TrypLE for 5 min at 37°C. NPSCs were incubated on gelatin (0.1%) for 1h at 37 °C to remove feeder cells. Then, NPSCs cells were rinsed with PBS −/− before being lysed using the iST kit (PreOmics GmbH, Planegg, Germany) following the manufacturer's instructions.

TSCs: 1-day prior lysis (4–5 days after seeding) TSCs were dissociated using TrypLE for 5 min at 37°C. TSCs were incubated on gelatin (0.1%) for 1h at 37 °C to remove feeder cells. TSC were plated overnight respectively on a 3 μg/mL vitronectin and 1 μg/mL laminin coated plate (1/1 ratio). The next day, cells were rinsed with PBS−/− before being lysed using the iST kit (PreOmics GmbH, Planegg, Germany) following the manufacturer's instructions.

The lysis day, another well of TSCs was dissociated using TrypLE for 5 min at 37°C. TSCs were incubated on gelatin (0.1%) for 1h at 37 °C to remove feeder cells. Then, TSCs cells were rinsed with PBS −/− before being lysed using the iST kit (PreOmics GmbH, Planegg, Germany) following the manufacturer's instructions.

PPSCs: The lysis day, PPSCs were dissociated using TrypLE for 5 min at 37°C. PPSCs were rinsed with PBS−/− before being lysed using the iST kit (PreOmics GmbH, Planegg, Germany) following the manufacturer's instructions.

The lysis day, another well of PPSCs was rinsed with PBS −/− before being lysed using the iST kit (PreOmics GmbH, Planegg, Germany) following the manufacturer's instructions.

EPSCs: The lysis day, EPSCs were dissociated using TrypLE for 5 min at 37°C. EPSCs were incubated on gelatin (0.1%) for 1h at 37 °C to remove feeder cells. Then, EPSCs were rinsed with PBS −/− before being lysed using the iST kit (PreOmics GmbH, Planegg, Germany) following the manufacturer's instructions.

Protein extraction and digestion

Samples were thawed and lysed (denatured, reduced and alkylated) for 10 min at 95°C and then Trypsin/LysC digested for 3h at 37°C. Purification of peptides was then carried out at room temperature on a spin cartridge, and peptides were finally eluted with the iST Fractionation Add-on (PreOmics GmbH, Planegg, Germany) in three fractions in 10μL of an LC-loaded buffer. Simultaneously, a protein assay has been realized to quantify proteins present in the samples. Once purified, the three fractions of each cell type (hNPSCs, hPSCs, hEPSCs and hTSCs samples) were prepared for mass spectrometry injection at approximatively 3μg of protein in 10μL.

Nanoliquid chromatography coupled with Tandem mass spectrometry (NanoLC-MS/MS)

The sample from Girard et al., 2023[48] were analyzed in Data-Dependent Analysis (DDA) and Parallel Accumulation Serial Fragmentation (PASEF) mode to generate the spectral library. Each sample of enzymatically digested plasma proteins (about 200 to 300ng) were separated on a 75μm × 250mm IonOpticks Aurora 3 C18 column (Ion Opticks Pty Ltd., Bundoora, Australia). A gradient of reverse phase buffer (Buffer A: 0.1% formic acid, 2% acetonitrile, 97.9% H_2O; Buffer B: 0.1% formic acid, 99,9% acetonitrile) was run on a nanoElute UHPLC System (Bruker Daltonik GmbH, Bremen, Germany) at a flow rate of 250 nL/min at 50°C controlled by HyStar software (v6.0.30.0, Bruker Daltonik). The liquid chromatography (LC) run lasted for 80min. A starting concentration of 2% buffer B increasing to 13% over the first 42 min was first performed and buffer B concentrations were increased up to 20% at 65min; 30% at 70min; 85% at 75min and finally 85% for 5min to wash the column. The temperature of the ion transfer capillary was set at 180°C. Ions were accumulated for 100ms, and mobility separation was achieved by ramping the entrance potential from −160V to −20V within 114ms. MS and MS/MS mass spectra were acquired with average resolutions 50.000 FWHM full width at half maximum (with an m/z range of 100–1700), respectively. To enable the PASEF method, precursor m/z and mobility information was first derived from full scan TIMS-MS experiments (with a mass range of m/z 100–1700). The quadrupole isolation width was set to 2 and 3 Th and, for fragmentation, the collision energies varied between 31 and 52 eV depending on the precursor mass and charge. TIMS, MS operation and PASEF were controlled and synchronized using the control instrument software OtofControl 6.2.5 (Bruker Daltonik). LC-MS/MS data were acquired using the PASEF method as des cribbed previously (Banliat et al., 2019) with a total cycle time of 1.31s, including 1 TIMS MS scan and 10 PASEF MS/MS scans. The 10 PASEF scans (100ms each) contained, on average, 12 MS/MS scans per PASEF scan. Ion mobility-resolved mass spectra, nested ion mobility vs. m/z distributions, as well as summed fragment ion intensities were extracted from the raw data file with DataAnalysis 6.0 (Bruker Daltonik).[72]

The three fractions per samples were then analyzed individually in diaPASEF mode. Each tryptic peptide sample, of approximately 400-500ng each, was analyzed under the same conditions as described above. These included the same analytical conditions (identical instrumentation, type of separation column and gradient length) and analysis on the same instrument (timsTOF Pro; Bruker Daltonik GmbH, Bremen, Germany)). For the development of the diaPASEF method, we used a method with an adapted instrument firmware to perform data-independent isolation of data from several 25 m/z wide precursor windows, also called segments, in a single TIMS separation (107.5ms). We used a method with two boxes per segment in each 107.5ms diaPASEF scan, i.e., a total of thirty-two segments and sixty-four boxes, of which sixteen of these scans perfectly cover the diagonal area of doubly and triply charged peptides in the m/z and ion mobility output range. MS and MS/MS data were collected over the m/z range 100–1700 and over the mobility range from 1/K0 = 0.6Vs.cm-2 to 1/K0 = 1.6Vs.cm-2. During each data collection, each TIMS cycle was 1.25 s long and comprised 1 MS and 22 cycles of diaPASEF MS/MS segments, comprising 2, 3 or 4 boxes, to cover a total of 64 boxes defined in the acquisition method. The collision energy was increased linearly with mobility from 68 eV at 1/K0 = 1.6Vs.cm-2 to 25 eV at 1/K0 = 0.6Vs.cm-2.

MS data processing

Ion mobility resolved mass spectra, nested ion mobility versus m/z distributions, and fragment ion intensity sums were extracted from the raw data file with DataAnalysis 6.0 (Bruker Daltonik). The signal-to-noise ratio was increased by summing the individual TIMS scans. Mobility peak positions and half-peak widths were determined on the basis of extracted ion mobilograms (EIM, ±0.05Da) using the peak detection algorithm implemented in the DataAnalysis software. Feature detection was also performed using DataAnalysis 6.0 software; stored at the raw data level.

Data analysis – Hybrid library generation

For the project library, the DDA raw files were analyzed in Spectronaut software version 16 (Biognosys, Schlieren, Switzerland), using the Pulsar search engine integrated into the Spectronaut software, and a search schema with default settings to generate respective spectral library. The calibration search was dynamic and MS1, MS2 correction factor was 1. Data were searched against the UniProt KB Human database (20,594 sequences, downloaded on February, 2023), with trypsin/P as the protease with up to one missed cleavage. To account for post-translational modifications and chemical labeling settings, carbamidomethylation of cysteine residues was defined as a fixed modification, and methionine oxidation and acetylation of Lysines and acetylation of protein N-termini were defined as variable modifications. An FDR less than 1% was ensured on precursor, peptide and protein level.

Additionally, the DIA files from the individual's samples, based on raw files, were searched in the same way as described above, to generate a combination of DDA and DIA in a so-called ''hybrid libraries''.

Library search of DIA data

The raw files from individual samples and acquired in DIA were then used again for the DIA analysis. The files were analyzed with Spectronaut using the previously generated hybrid libraries and default settings, and allowed quantification of the precursors, peptides and proteins. The results were filtered by a 1% FDR on precursor, peptide and protein level using a target-decoy approach, which corresponds to a Q value $\leq$ 0.01[73]

Quantification data were then normalized by Spectronaut software to take into account the overall acquisition heterogeneity between samples. Given the number of samples analyzed (less than 500 individuals), the type of data normalization carried out for the whole dataset was a local regression normalization described by Callister et al. 2006.

The LC-MS data, libraries, results tables and Spectronaut projects of the different analysis have been deposited to the ProteomeXchange Consortium[74] via the PRIDE[75] partner repository with the dataset identifier PXD043712. The Spectronaut projects can be viewed using the free Spectronaut viewer (www.biognosys.com/technology/spectronaut-viewer). The data used for the figures are available in Table S4.

QUANTIFICATION AND STATISTICAL ANALYSIS

Statistics

For differential gene expression analysis, P-values were adjusted based on an alpha threshold of 0.1.

For MAplots, pvalues were re-used from differential gene expression analysis. Genes with a pvalue under 0.05 and a log fold change superior to 2 or inferior to 2 were printed, except for the comparison between naive pluripotent stem cells versus primed pluripotent stem cells, where the number of upregulated genes was low enough to be printed.

For Boxplots, pvalues were re-used from differential gene expression analysis. Asterisks indicate statistical significance of the difference compared to PPSCs: *pvalue <0.05.

For 5mC quantification analysis, significance levels were determined using a Kruskal Wallis test, followed by a Dunn comparison. Asterisks indicate statistical significance of the difference: * pvalue <0.05.

DGE-seq data preprocessing

Read pairs used for analysis matched the following criteria: all 16 bases of the first read had quality scores of at least 10 and the first 6 bases correspond exactly to a designed well-specific barcode. The second reads were aligned to RefSeq human mRNA sequences (hg19) using bwa version 0.7.17. Reads mapping to several transcripts of different genes or containing more than 3 mismatches with the reference sequences were filtered out from the analysis. DGE profiles were generated by counting for each sample the number of unique UMIs associated with each RefSeq genes. DGE-sequenced samples were acquired from 8 sequencing runs. Samples were retained if the number of UMIs was superior to 50000 and the number of expressed genes above 6000, a total of 386 samples passed those cutoffs. Also, genes have been filtered by keeping only a set of over-dispersed genes determined. To pick these, the co-efficient of variation of each gene from the normalized adjusted expression was fitted by the mean expression of each gene, using a LOESS method. Genes with a positive residual for the regression were marked as over-dispersed. This leads to a total of 23885 genes.

Transcriptomic analyses

The 8 runs were merged using ComBat[76] (Leek et al. 2022) from the R library "sva". Technical replicates between batches were used as references for batch-effect correction, but only samples from 4 runs were kept the others are out of the scope of this article. Each gene expression of the corrected values was subtracted by the minimum of the gene expression before the batch correction. This step does not change the relative expression of genes; however, it permits an easier interpretation of the expression values as minimums cannot be less than zero. Finally, each set of technical replicates were merged. The data used for the figures are available in Table S2.

Heatmaps were computed using complexheatmap R package (2.6.2)[77,78]; samples were clustered from the Euclidean distance of expression by a hierarchical clustering using Ward's method. Differential gene expression analysis was performed with deseq2 R package (1.34.0)[79] in combination with log fold change shrinkage function from apeglm R package (1.16.0).[80] Deseq2 was used with raw counts expression matrix and the corresponding design was cell type plus the run information. P-values were adjusted based on an alpha threshold of 0.1.

MAplots was constructed with "ggmaplot" function from ggpubr R package (0.4.0), name of genes was printed if the genes have an adjusted pvalue under 0.05 and a log fold change superior to 2 or inferior to 2, except for the comparison between naive pluripotent stem cells versus primed pluripotent stem cells, where the number of upregulated genes was low enough to be printed. Boxplots were computed with ggplot R package (3.3.3) and pvalues were re-used from differential gene expression analysis.

ADDITIONAL RESOURCES

No additional resources.